INL/EXT-18-45212
Revision 0

Light Water Reactor Sustainability Program

Enhancement of the Structural Health Monitoring Framework by Optimizing Vibro-Acoustic Modulation Technique to Localize Alkali-Silica Reaction Degradation in Medium-Sized Concrete Samples

April 2018

U.S. Department of Energy
Office of Nuclear Energy

DISCLAIMER

This information was prepared as an account of work sponsored by an agency of the U.S. Government. Neither the U.S. Government nor any agency thereof, nor any of their employees, makes any warranty, expressed or implied, or assumes any legal liability or responsibility for the accuracy, completeness, or usefulness, of any information, apparatus, product, or process disclosed, or represents that its use would not infringe privately owned rights. References herein to any specific commercial product, process, or service by trade name, trade mark, manufacturer, or otherwise, does not necessarily constitute or imply its endorsement, recommendation, or favoring by the U.S. Government or any agency thereof. The views and opinions of authors expressed herein do not necessarily state or reflect those of the U.S. Government or any agency thereof.

INL/EXT-18-45212

Light Water Reactor Sustainability Program

Enhancement of the Structural Health Monitoring Framework by Optimizing Vibro-Acoustic Modulation Technique to Localize Alkali-Silica Reaction Degradation in Medium-Sized Concrete Samples

Sankaran Mahadevan
Sarah Miele
Pranav Karve
Julia Finfrock
Vivek Agarwal
Eric Giannini

April 2018

Idaho National Laboratory
Idaho Falls, Idaho 83415
Vanderbilt University
Nashville, Tennessee 37235
RJ Lee Group
Monroeville, Pennsylvania 15146
http://www.inl.gov

Prepared for the
U.S. Department of Energy
Office of Nuclear Energy
Under DOE Idaho Operations Office
Contract DE-AC07-05ID14517

ABSTRACT

Assessment and management of aging concrete structures in nuclear power plants require a more systematic approach than simple reliance on existing code margins of safety. Health monitoring of concrete structures is performed to understand the current condition of a structure based on heterogeneous measurements and then produce high-confidence actionable information regarding structural integrity. This information can then be used to support operational and maintenance decisions.

The objectives of this ongoing research project focus on health monitoring and data analytics of concrete slabs containing reactive aggregates and thus subjected to degradation due to alkali-silica reaction (ASR). A controlled concrete slab with four pockets of reactive aggregates (pure silica, wells, placitas, and spratt) was cast at Vanderbilt University and cured in representative conditions to accelerate degradation due to ASR. A set of four concrete samples were also cast and cured at the University of Alabama for ASR testing. Of these four samples, two slabs contained reactive aggregates while the other two had the non-reactive aggregate counterparts mixed throughout the samples. Vibro-acoustic methods were used on these slabs to locate large pockets of ASR within the reactive samples and determine the effects of rebar using the non-reactive slabs.

Vibro-acoustic modulation (VAM) is a vibration-based nondestructive examination (NDE) method that utilizes signatures of nonlinear dynamic interactions on contact surfaces of crack or delamination damage to detect and localize the damage. VAM analysis was conducted on both Vanderbilt University and University of Alabama samples using multiple variables for damage detection and localization. The results from the data analysis of the NDE vibro-acoustic techniques on concrete slabs cured at Vanderbilt University and the University of Alabama are discussed in detail in this report. The major outcome of the analysis suggests that the VAM method can be used to detect damage within the concrete samples by comparing the results found in different sections of the samples. Results for damage localization are dependent on multiple variables used in the VAM experiments.

Digital image correlation (DIC) is a three-dimensional, full-field, optical NDE technique to measure contour, deformation, vibration, and strain. The application of the DIC technique to study ASR-related degradation on a large concrete sample at the University of Tennessee, Knoxville, is discussed and observations are presented in this report.

EXECUTIVE SUMMARY

One challenge facing the current fleet of light water reactors in the United States is age-related degradation of their passive assets, including concrete, cables, piping, and the reactor pressure vessel. As the current fleet of nuclear power plants (NPPs) continues to operate for 60 years or more, it is important to understand the current and the future condition of passive assets under different operating conditions that would support operational and maintenance decisions. To ensure safe and reliable long-term operation of the current fleet, the United States Department of Energy's Office of Nuclear Energy funds the Light Water Reactor Sustainability Program to develop the scientific basis for extending the operation of commercial light water reactors beyond the current license extension period.

Among the different passive assets of interest in NPPs, concrete structures are investigated in this research project. Reinforced-concrete structures found in NPPs can be grouped into the following categories: (1) primary containment, (2) containment internal structures, (3) secondary containments/reactor buildings, and (4) spent fuel pool and cooling towers. These concrete structures are affected by a variety of degradation mechanisms that are related to chemical, physical, and mechanical causes and to irradiation. Age-related degradation of concrete results in gradual microstructural changes (e.g., slow hydration, crystallization of amorphous constituents, and reactions between cement paste and aggregates). The purpose of structural health monitoring of concrete is to assess the current condition of a structure and to provide high-confidence actionable information regarding structural integrity and reliability. Vanderbilt University, in collaboration with Idaho National Laboratory and Oak Ridge National Laboratory, is developing a probabilistic framework for structural health monitoring and managing the condition of aging concrete structures in NPPs. This integrated framework includes four elements: (1) monitoring, (2) data analytics, (3) uncertainty quantification, and (4) prognosis.

The objective of this continuing research project is to obtain degradation data for concrete structures from a series of experiments conducted under controlled laboratory conditions. The ability of nondestructive examination (NDE) methods to characterize concrete deterioration and correlate it with structural performance is also being assessed. This report focuses on concrete degradation caused by alkali-silica reaction (ASR). Concrete specimens were prepared to develop accelerated ASR degradation in a laboratory setting. NDE techniques, which include thermography, mechanical deformation measurements, nonlinear impact resonance-acoustic spectroscopy, and vibro-acoustic modulation (VAM), were previously used to detect the damage caused by ASR on concrete slabs cured at Vanderbilt University, and documented in an earlier report. The current report focuses on damage localization using the VAM technique and investigates the effect of different characteristics of the VAM tests on the damage localization results. The same investigation is also carried out for four concrete slabs acquired from the University of Alabama, where the reactive aggregates are dispersed throughout two of the samples.

Some of the outcomes of these experiments are as follows:

1. A 24 × 24 × 6 in. concrete slab cast at Vanderbilt University with four different types of reactive aggregate and aggressively cured to produce accelerated ASR degradation is analyzed. The impacts of ASR development on the test specimen were examined using VAM.
2. Analysis for detection and localization of ASR in 12 × 24 × 12 in. concrete slabs cast and cured at the University of Alabama with different reactive and non-reactive aggregates was conducted using VAM techniques.
3. The digital image correlation is an ongoing study of a large concrete specimen constructed at University of Tennessee, Knoxville. The researchers have collected eight sets of data tracking the deformation of the specimen due to ASR.

The experiments and outcomes described in this milestone report are focused on concrete structural monitoring measurements and data analytics. This will support continuous assessment of concrete performance and enhance the structural health framework.

ACKNOWLEDGMENTS

This report was made possible through funding by the United States Department of Energy's Light Water Reactor Sustainability Program. We are grateful to Alison Hahn of the United States Department of Energy and Bruce Hallbert and Craig A. Primer at Idaho National Laboratory for championing this effort. We also thank Jodi Vollmer and Dawn Davidson at Idaho National Laboratory for technical editing and formatting of this report.

CONTENTS

FIGURES

TABLES

ACRONYMS

ASR	alkali-silica reaction
DEMEC	demountable mechanical strain gauge
DIC	digital image correlation
LS	linear spectrum
NDE	nondestructive examination
NPP	nuclear power plant
PSD	power spectral density
SBSum	sideband sum
SHM	structural health monitoring
UTK	University of Tennessee, Knoxville
VAM	vibro-acoustic modulation

Enhancement of the Structural Health Monitoring Framework by Optimizing Vibro-Acoustic Modulation Technique to Localize Alkali-Silica Reaction Degradation in Medium-Sized Concrete Samples

1. INTRODUCTION

The majority of existing nuclear power plants (NPPs) continue to operate beyond their initial licensed life expectancy. The passive structures, systems, and components of NPPs as they continue to operate suffer deterioration that affects structural integrity and performance. Monitoring the condition of these elements of an NPP is essential for ensuring that their conditions meet performance and safety requirements over the entire expected plant lifespan. This project focuses on concrete structures in NPPs. The concrete structures are grouped into the following categories: (1) primary containment, (2) containment internal structures, (3) secondary containment/reactor buildings, and (4) other structures such as used fuel pools, dry storage casks, and cooling towers. These concrete structures are affected by a variety of chemical, physical, and mechanical degradation mechanisms, such as alkali-silica reaction (ASR), chloride penetration, sulfate attack, carbonation, freeze-thaw cycles, shrinkage, and mechanical loading (Naus 2007). The age-related deterioration of concrete results in continuing microstructural changes (e.g., slow hydration, crystallization of amorphous constituents, and reactions between cement paste and aggregates). Therefore, it is important that changes over long periods of time are measured and monitored, and that their impacts on the integrity of the components are analyzed to best support long-term operations and maintenance decisions of the existing fleet of nuclear reactors.

Structural health monitoring (SHM) can produce actionable information regarding structural integrity that, when conveyed to the decision-maker, enables risk management with respect to structural integrity and performance. The SHM methods and technologies include assessment of critical measurements, monitoring, and analysis of aging concrete structures under different operating conditions. In addition to data from the specific system being monitored, information may also be available for similar or nominally identical systems in an operational NPP fleet, as well as legacy systems. Therefore, to take advantage of this valuable information, Christensen (1990) suggested that assessment and management of aging concrete structures in NPPs require a more systematic and dynamic approach than simple reliance on existing code margins of safety.

Through the Light Water Reactor Sustainability Program, national laboratories (Idaho National Laboratory and Oak Ridge National Laboratory) and universities (Vanderbilt University, University of Nebraska-Lincoln, University of Alabama, University of South Carolina, and Georgia Tech University) have begun research on concrete SHM techniques. This report focuses on the collaboration between national laboratories and Vanderbilt University in researching concrete SHM in accordance with the proposed framework discussed in Mahadevan et al. (2014). The goal of this research is to enable plant operators to make risk-informed decisions on structural integrity, remaining useful life, and performance of concrete structures across the NPP fleet. The project long-term research objective is to produce actionable information regarding structural integrity that is individualized for a structure of interest and its performance goals. In addition, the project supports the research objectives of three pathways under the Light Water Reactor Sustainability Program (i.e., the Advanced Information, Instrumentation, and Control Systems Technologies Pathway; Materials Aging and Degradation Pathway; and Risk-Informed Safety Margin Characterization Pathway).

Vanderbilt University, in collaboration with Idaho National Laboratory and Oak Ridge National Laboratory, is developing a framework for evaluating and forecasting the health of aging NPP concrete structures that are subject to physical, chemical, and mechanical degradation (Mahadevan et al. 2014; Agarwal and Mahadevan 2014). The framework will investigate concrete structure degradation by integrating the following technical elements: (1) health condition monitoring, (2) data analytics, (3) uncertainty quantification, and (4) prognosis. For details on each element of the proposed framework, refer to Mahadevan et al. (2014). The framework will help plant operators make risk-informed decisions on structural integrity, remaining useful life, and concrete structure performance. The demonstration performed at Vanderbilt University using various techniques to assess ASR degradation in controlled concrete specimens was reported in Mahadevan et al. (2016, 2017).

The objective of this report is to examine the use of two techniques in informing the prognostics and health management framework, namely, vibro-acoustic modulation (VAM) and digital image correlation (DIC). A series of experiments were conducted at the Vanderbilt University to provide sufficient degradation data in support of the prognostics and health management framework (Mahadevan et al. 2014; Mahadevan et al. 2016) to examine and forecast the condition of aging concrete structures in NPPs. Within this experimental campaign, multiple concrete slab samples are exposed to different accelerated aging conditions in a laboratory to ensure formation of ASR gel within an observable timeframe. These concrete samples also differ in sizes and types of embedded aggregates. The above-mentioned VAM and DIC techniques are used to detect and assess the ASR-induced damage in these concrete samples over an extended period of time.

The technical background, experimental setting, data processing, significant results, technical findings, and conclusion are included in the remainder of this report, which is organized as follows:

- Section 2 discusses the technical basics of the ASR development and the VAM and DIC techniques used to assess the effects of ASR on the integrity of concrete samples developed at the Vanderbilt University.
- Section 3 describes the various concrete specimens exposed to different ASR accelerated degradation conditions and the laboratory experimental setup of the VAM and DIC techniques.
- Section 4 describes the data analysis methods applied to the collected monitoring VAM data and presents the significant technical findings.
- Section 5 describes the data analysis methods applied to the DIC data and presents the significant technical findings
- Section 6 discusses the research summary and future activity.

2. TECHNICAL BACKGROUND

2.1 Development and Impact of Alkali-Silica Reaction

ASR is a reaction in concrete between the alkali hydroxides (K+ and Na+) in the pore solution and the reactive non-crystalline (amorphous) silica (S2+) found in many common aggregates, given sufficient moisture. This reaction occurs over time and causes the expansion of the altered aggregate by the formation of a swelling gel of calcium silicate hydrate (C-S-H). Reactive silica is mainly provided by reactive aggregates and the alkalis by the cement clinker. ASR swelling results from the relative volume increase between the product and reactant phases involved in the chemical reaction. First, the products expand in pores and micro-cracks of the cementitious matrix. Once this free expansion space is filled, the swelling is restrained, and the product phases exert local pressure on the surrounding concrete skeleton (Ulm et al. 2000). Figure 1 depicts the mechanism of ASR (Kreitman 2011).

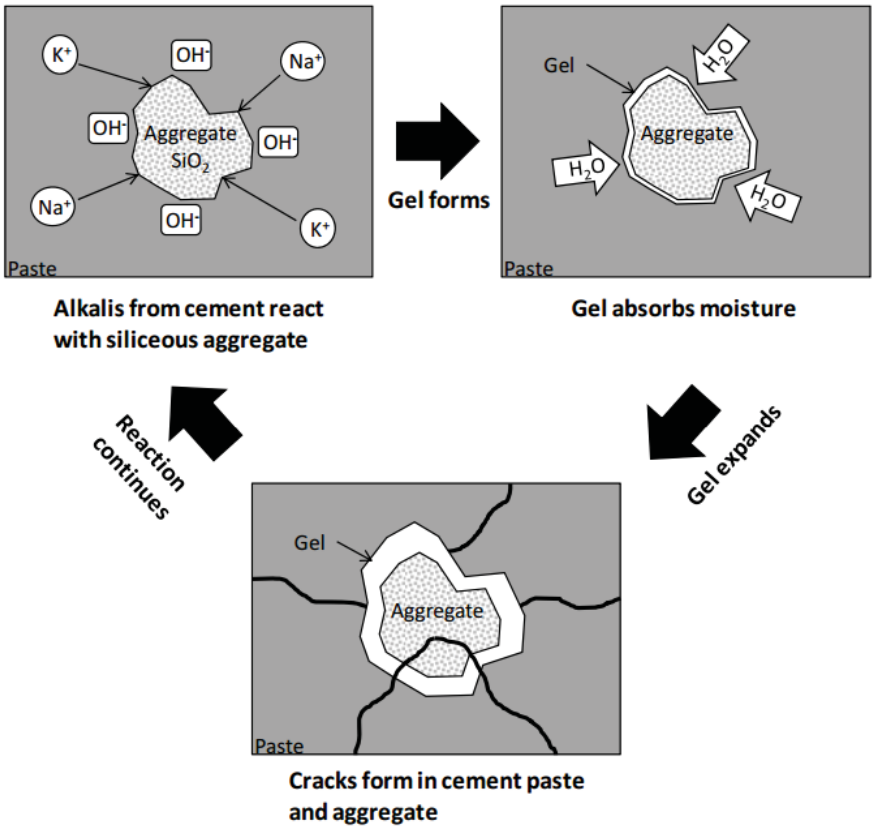

Figure 1. Mechanism of ASR (Kreitman 2011).

With water presence, the ASR gel increases in volume and exerts an expansive pressure inside the material, causing spalling micro- to macro-cracks (due to nonhomogeneous swelling related to non-uniform moisture distribution). As a result, ASR reduces the stiffness and tensile strength of concrete, because these properties are particularly sensitive to micro-cracking. ASR also can cause serious cracking in concrete, resulting in critical structural problems that can even force the demolition of a particular structure. The serviceability of concrete structures includes the resistance to excessive deflections, as well as a host of other durability concerns that can shorten the service life of a structure. Large surface crack widths and deep penetration of open surface cracks promote ingress moisture and any dissolved aggressive agents, such as chlorides. Additionally, the loss of concrete stiffness and potential for reinforcement yield are concerns for concrete deflection capabilities.

ASR is a complex chemical phenomenon, the rate and extent of which depend on a number of material and environmental parameters, for which the interactions among parameters is not fully understood. This critical nature of ASR on premature concrete deterioration requires the quantitative assessment of ASR structural effects during service life (both in time and space). In particular, a combined experimental modeling investigation method is required to evaluate the impact of ASR on the dimensional stability of concrete structures. Although ASR has been identified as a cause of deterioration of numerous concrete structures and research has yielded some understanding of the mechanism of the reaction, the structural effects of ASR and how to best assess the extent of damage to existing structures remain major topics of ongoing research. This is because the expansion and cracking patterns (the most obvious sign of distress) caused by ASR affect both the concrete and the reinforcing steel, but similar crack patterns can also be produced by other distress mechanisms (i.e., drying shrinkage and sulfate attack).

In the nuclear industry, a scoping study of ASR in concrete is performed to support future activities that include evaluating the effects of ASR on the structural capacity. From a safety perspective, the remaining capacity of a structure exhibiting distress due to ASR is an important factor in operational and maintenance management decisions. This is a challenging task for various reasons. First, the extent of the degradation will vary throughout the element as a function of the moisture content and as a function of the degree of restraint provided by the steel reinforcement. Also, it may be difficult to predict the properties of the concrete using certain testing results taken from the structure, because the size of the defects caused by the ASR may be large compared to a small structure, such as the cylinder (resulting in anomalously low tested strength), but the defects are small compared to the larger structure (suggesting there may be sufficient capacity). In addition, there is no reliable nondestructive means of estimating the degree of the reaction in an existing concrete structure.

ASR can potentially affect concrete properties and performance characteristics, such as compressive strength, the modulus of elasticity, flexural stiffness, shear strength, and tensile strength. ASR can also impact material properties, but the structural performance of concrete elements depends on whether or not the concrete is unconfined or confined within reinforcing bars. The concrete core testing was conducted at the Seabrook Station NPP in February 2011 as part of the license renewal submission (NextEra Energy Seabrook 2012). These tests confirmed the presence of ASR-induced cracks in various structures within the plant and reduced modulus to some extent. The impact of reduced modulus on ASR-affected structures was evaluated. This evaluation found that the overall structure integrity was still within the strength requirements.

2.2 Damage Evaluation Techniques for Monitoring Alkali-Silica Reaction

Multiple types of SHM techniques have been studied for detecting ASR damage in concrete structures. They are broadly categorized as contact monitoring techniques and non-contact monitoring techniques. The contact monitoring techniques include mechanical deformation measurement, acoustic emission, ultrasonic detection, nonlinear impact resonance-acoustic spectroscopy, VAM, and diffuse wave spectroscopy. The non-contact monitoring techniques include DIC and infra-red thermography imaging. The standard test methods for determining the potential alkali-silica reactivity and for determining the amount of time needed for concrete to change due to ASR are documented in ASTM C1567-13, “Standard Test Method for Determining the Potential Alkali-Silica Reactivity of Combinations of Cementitious Materials and Aggregate (Accelerated Mortar-Bar Method),” and ASTM C1293-08b, “Standard Test Method for Determination of Length Change of Concrete due to Alkali-Silica Reaction,” respectively. Earlier reports by Mahadevan et al. (2016, 2017) have studied various techniques and found them to be useful in damage detection. The VAM technique shows particular promise in damage localization and is investigated in detail in this report. In addition, the DIC technique is investigated in detail with respect to the large sample at the University of Tennessee, Knoxville (UTK). A brief overview of the VAM and DIC techniques is given below.

2.2.1 Vibro-Acoustic Modulation

VAM, also known as nonlinear wave modulation spectroscopy, is a nondestructive examination (NDE) technique that relies on detecting dynamic signature of nonlinear structural behavior as the primary indicator of damage. Specifically, VAM aims at detection of modulation of a higher frequency by a lower frequency caused by delamination or cracks in structural components. The utility of VAM for detecting debonding flaws and cracks in composites, metals, as well as ASR-induced cracks in concrete (Chen et al. 2008, 2009), has been demonstrated in the past.

In a VAM technique, the structural component of interest is excited simultaneously using a combination of two signals of specific frequencies, and the dynamic response is measured at various locations using acoustic sensors (accelerometers). The low-frequency input is termed the "pump," and the high-frequency input is termed the "probe" (Kim et al. 2014). The geometric or material nonlinearity in the form of variable contact area or nonlinear adhesive bond at the surfaces of a crack or a delamination causes modulation of the probing frequency by the pumping frequency. This modulation, and hence the presence of the flaw, can be seen in the frequency spectra of measured response as peaks of higher magnitude (sidebands) around the probe frequency. The interaction of these signals at different frequencies is used to understand the nonlinear stress-strain relationship in the structure of interest. For example, Figure 2 shows the response when the two excitation signals are theoretically applied to a structure. If the structure is linear and damped, the response in the steady state is the linear superposition of the responses of each signal, and only the linear components of Figure 2 will appear in the frequency spectrum of the response. Damage in a structure introduces nonlinearity and as a result, the response contains both the probing frequency and the pumping frequency in addition to other frequency components such as harmonics of each signal and sidebands around the probing signal as shown in Figure 2. Most of the previous work on VAM tests has focused on detection of damage based on the presence of sidebands in the spectrum of dynamics response of the structure. Recently, Singh et al. 2017 showed that a VAM test can be used for damage localization or damage mapping. They hypothesized that the effect of (geometric or material) nonlinearities is pronounced near the location of the flaw, and hereafter, the relative magnitude of a sidebands-based damage index may enable localization of the flaw. That is, if the spatial distribution showing the variation of the damage index is obtained using a sensor grid, the damage is located in the neighborhood of sensors exhibiting higher magnitude of the damage index. They tested their hypothesis using numerical simulations of VAM in delaminated composite plates. They studied damage indices based on various characteristics of spectrum of the dynamic response (magnitude of sidebands, probe frequency, pump frequency) of the plate and established the feasibility of VAM-based damage localization. Thus, the utility of the damage mapping scheme has been studied for homogeneous, anisotropic, thin composite plates by performing numerical experiments. However, the applicability of VAM-based damage mapping to detect and localize cracks in structural concrete components has not been investigated. We remark that thick, heterogeneous structural concrete components present significant challenges for VAM test setup, data analytics, and damage mapping. In this report we discuss our experimental investigation into various aspects of ASR-induced damage (crack) localization for concrete components using VAM testing.

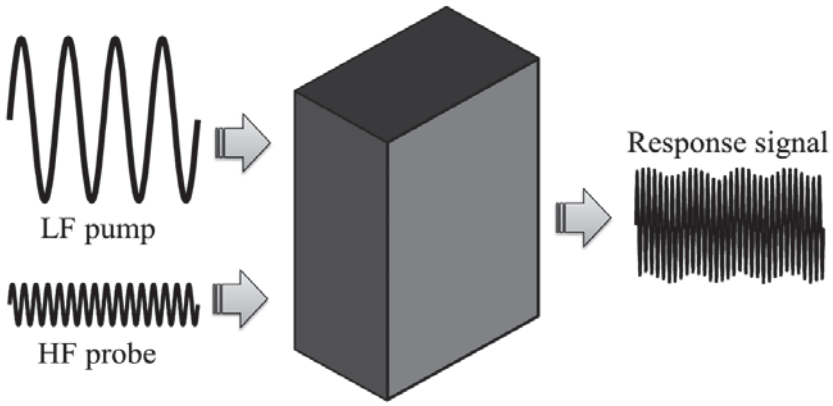

Figure 2. The principal of the VAM technique (Kim et al. 2014).

2.2.2 Digital Image Correlation

DIC is an optical non-contact NDE technique that is capable of measuring the deformation, displacement, and strain of a structure (Bruck, Esselman, and Fallin 2012). During NPP routine pressure tests on containment vessels, when the internal pressure reaches 60 psi, it might be possible to use DIC to determine deformation of the concrete containment. DIC is capable of detecting surface defects, such as cracks, micro-cracks, and spalling, but it is unable to detect any subsurface defects. The primary benefit of DIC is in measuring deformation; therefore, the ability of DIC to detect changes in the dimensions of the slab due to ASR gel expansion is of interest in this study. DIC requires a speckled pattern on the specimen to anchor observations at different points in time. This also presents a problem for the cement brick specimens that are immersed in a sodium hydroxide solution or water; the pattern is disturbed and partly dissolved in the sodium hydroxide solution. However, if the cement brick specimen is cured above water, DIC might be applicable.

3. CONCRETE SAMPLES

In this work, we investigate the utility of the SHM techniques discussed in Section 2.2 for monitoring degradation in concrete samples due to ASR. The monitoring techniques are studied with concrete samples constructed and cured in the laboratory. These include a medium-sized concrete slab (without reinforcement) with pockets of reactive aggregate cast and cured at Vanderbilt University, Nashville, Tennessee, a large reinforced concrete slab with reactive aggregates cast and cured at UTK, and concrete blocks (without reinforcement) with reactive and non-reactive aggregates cast and cured at the University of Alabama, Tuscaloosa, Alabama.

3.1 Medium-Sized Concrete Slab at Vanderbilt University

In this section, we discuss a medium-sized concrete slab of dimensions of 2 ft × 2 ft × 6 in. casted on December 21, 2015, and cured at Vanderbilt University. The details on casting and curing process of this concrete sample is discussed in detail in the report by Mahadevan et al. (2016). Figure 3 shows an image of the slab immediately after the mold was removed.

Figure 3. 2 ft × 2 ft × 6 in. dimension concrete slab.

Four types of aggregate were placed in pockets at a depth of 3 in. in the four quadrants of the slab (Figure 4). The aggregates were placed in pockets instead of being dispersed throughout the slab so that the reactivity of each aggregate can be determined independently. Additionally, since the locations of the pockets of aggregate are known, this information was used to validate the localization of ASR from monitoring perspective. The four types of aggregates used are as follows:

1. Pure silica—powder from local ceramic shop
2. Wells—coarse aggregate from Wells, Maine, donated by the University of Alabama

3. Placitas—coarse aggregate from Placitas, New Mexico, donated by the University of Alabama
4. Spratt—coarse aggregate from Spratt quarry in Ontario, Canada, donated by the Ontario Ministry of Transportation.

From December 21, 2015, to September 2016, the medium-sized concrete slab did not show visual signs of degradation due to ASR. In October 2016, first visual evidence of degradation due to ASR was observed. Since then, the degradation-related damage has become increasingly pronounced. The first indication of damage was detected by two vibration-based techniques, nonlinear impact resonance-acoustic spectroscopy and VAM. Then, hairline cracks were observed on the surface of the slab, and later, an ASR gel effluent and whitish powder seeped out of the slab. In Figure 4, the red squares identify the locations where seepage of ASR gel effluent was observed on the sides of the slab. The seepage corresponding to locations marked in red squares in Figure 4 is shown in Figure 5, Figure 6, and Figure 7, respectively.

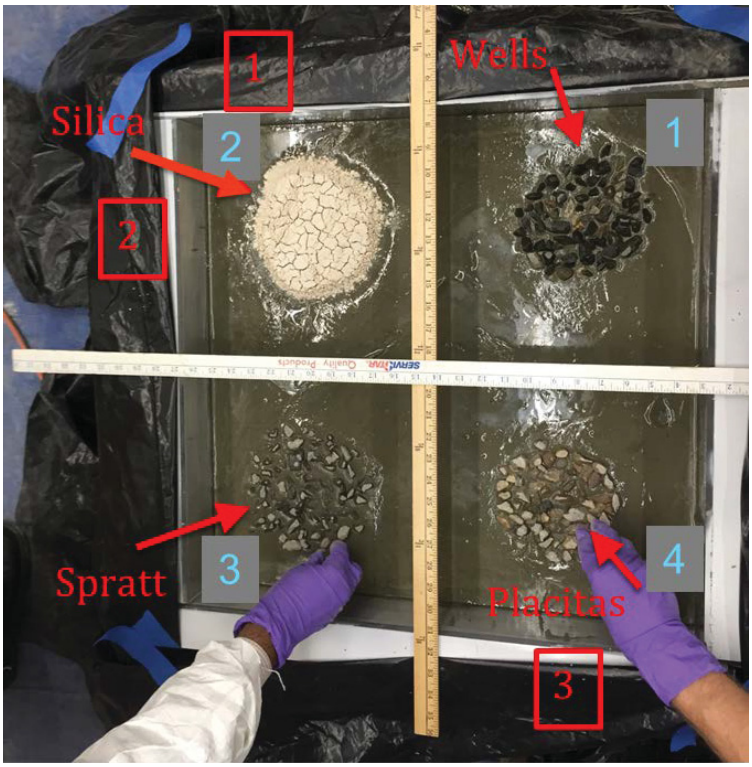

Figure 4. Pockets of aggregate in the slab during casting with red squares identifying visually observed cracks and effluence on the side of the slab.

Figure 5. Damage location 1—cracking and powder effluence.

Figure 6. Damage location 2—clear gel effluence.

Figure 7. Damage location 3—cracking and powder effluence.

The whitish powder or gel effluents detected in Figure 5, Figure 6, and Figure 7 (the figure captions indicate whether powder or gel was observed) were tested with inductively coupled plasma-optical emission spectroscopy at the Vanderbilt University Civil and Environmental Engineering Laboratory and it was confirmed that the substance was ASR gel (see Mahadevan et al. 2017 for details).

3.2 Concrete Slabs Cast and Cured at the University of Alabama

A set of four samples were received from the University of Alabama for ASR testing. These four samples are 12 × 24 × 12 in. in dimension. Two slabs contained reactive aggregates while the other two had the non-reactive aggregate counterparts mixed through the samples. All samples were cured together using the same environmental factors. All samples also contained rebar throughout. In using mechanical deformation testing, it was shown that both the reactive samples increased in size and showed cracking, unlike the non-reactive samples that did not.

3.3 Large Concrete Slab at the University of Tennessee, Knoxville

Vanderbilt University began performing DIC in late August 2016 on an ASR mockup concrete slab at UTK. Three slabs of dimensions X × Y × Z were cast in 2016 and the progression of ASR will be studied over 3 years with a variety of monitoring techniques. For details on the UTK concrete slab, refer to the report [Z. Ma et al., 2016]. A black-background-white-speckle pattern using acrylic latex paint was applied to the slab for DIC analysis. Figure 8 displays a 2 × 2 ft area of interest on the large slab.

Figure 8. DIC camera support installation over the area of interest.

4. LABORATORY TESTS FOR DAMAGE DETECTION AND LOCALIZATION

In this section, we discuss application of two monitoring techniques, namely VAM and DIC, in assessing the health of the concrete samples degraded due to ASR. VAM is used for ASR-induced damage detection and localization in the medium-sized concrete slab cast at Vanderbilt University (referred to as VU slab) and the slabs from the University of Alabama (referred to as Alabama slabs). DIC is used to detect ASR damage through strain measurements, in the large slab cast at UTK (referred to as the UTK slab).

4.1 Vibro-Acoustic Modulation Experimental Setup

VAM is a vibration-based method that utilizes signatures of nonlinear dynamic interactions on contact surfaces of cracks or delamination damage to detect and localize the damage. To the best of our knowledge, the applicability of VAM tests in detecting and localizing ASR-induced damage (cracks) has not been studied in the laboratory. As a part of this research project, VAM tests are conducted on the medium-sized slab with reactive aggregate pockets at known locations, as well as on four concrete blocks cast using either reactive or non-reactive aggregates. In this section, we discuss our findings.

The nonlinear dynamic interactions at the surfaces of a crack, or a delamination can be induced using either an impact or VAM technique. In the impact modulation mode, the impact-induced vibrations of the structure modulate a higher frequency at the damage interface to produce a dynamic signature of the nonlinearity. In our previous work, we tested this approach, but these experiments failed to produce clear

indicators of nonlinearity in a specimen with ASR damage. Therefore, we use the VAM technique for all the experiments reported. In the VAM technique, the structural component of interest is excited using a lower "pump" frequency and a higher "probe" frequency. Nonlinear behavior at the interface (variable contact area or nonlinear adhesive bond at the interface) causes modulation of the probe frequency by the pump frequency. This can be seen as sidebands around the probe frequency in the spectra of measured response in a VAM test. In our laboratory experiments, we deliver the pump and probe excitations using piezo-stack actuators. We vary the locations of these actuators, as well as the frequencies at which they operate (i.e., the pump and probe frequencies). We measure the response of the structural component of interest using a finite number of accelerometers placed on the surface of the component. The relative magnitudes of sidebands at various accelerometer locations are used to map the damage (ASR-induced cracks) in the component. The performance of the VAM test depends on the values of parameters used, as well as on the methodology used for processing the data collected during a VAM test. We discuss, next, various factors involved in the selection of test parameters (pumping frequency, probing frequency) and data processing methods (noise reduction, sideband detection).

4.1.1 Pumping Frequency

In our laboratory experiments, we used the first fundamental frequency of the slab as well as an arbitrary low frequency as the pumping frequency, denoted as f_{pu}. We estimated the fundamental frequency of the structural component by conducting a hammer test. That is, we excited the structural component using an impact hammer and measured the acceleration at various locations using accelerometers. We computed the power spectral density (PSD) of the measured acceleration time series using the Welch's method (Welch, 1967). The PSD shows multiple peaks that correspond to natural frequencies of the structure. The first and most prominent peak was assumed to be first modal frequency. For Vanderbilt University's medium-sized slab, this value was 920 Hz. The frequency of 920 Hz was used as f_{pu} for this slab for all our experiments. For the University of Alabama samples, 920 Hz was used as an arbitrary low f_{pu}, in addition to the first modal frequencies for each sample. The modal frequencies for the University of Alabama samples found using a hammer test are listed in Table 1.

Table 1. Experimental first modal frequency for each sample.

Slab Sample	Approximate First Modal Frequency (Hz)
Vanderbilt University medium slab	920
University of Alabama—Gold Hill reactive	1865
University of Alabama—Gold Hill control (non-reactive)	2390
University of Alabama—Grand Junction reactive	1695
University of Alabama—Grand Junction control (non-reactive)	2240

4.1.2 Probing Frequency

It has been reported in the literature that the probing frequency, denoted as $\boldsymbol{f_{pr}}$, should be at least 10 to 20 times the pumping frequency (Singh et al. 2017). When the $\boldsymbol{f_{pr}}$ is *N* times the pumping frequency it allows for the crack to open and close N times in a pumping cycle. Thus, the ratio between the pump and probe decides the opportunity (number of times per cycle of pumping vibrations) for modulation to occur. In accordance with these guidelines, $\boldsymbol{f_{pr}}$ ranging from 17 to 21 kHz were used in our experiments. The amplitude and location of the probing signal was also varied in different experiments.

In numerical studies the f_{pr} worked best for damage localization when it was 1/10th the amplitude of the f_{pu}. In general, this is true for our experiments. The acceleration spectra plots do not show this clearly, because the ordinates of the spectra are multiplied by the square of the circular frequency. However, in linear spectra of displacements, the strength of the probing signal is always less than the

strength of the pumping signal. In our experiments, the pump and probe signal amplitudes were controlled by signal (function) generators. We used four amplitudes for the output voltage of the probing signal generator—500, 250, 100, or 50 mV. The output voltage of the pumping signal generator was maintained at 500 mV. The pumping and probing signals were amplified by an amplifier and sent to the piezo-stack actuator. A constant amplification factor (+28 dB) was maintained for all tests.

4.1.3 Accelerometers

A maximum of 12 accelerometers were placed on the concrete specimen at a time and connected to the data acquisition system. The locations of these accelerometers were varied for each experiment. The accelerometers were calibrated biweekly to ensure accuracy. Calibration was performed by applying excitations directly to the accelerometer using a PCB Piezotronics handheld shaker and ensuring that the accelerometer reading was close the shaker output. Minor differences in the shaker and accelerometer readings were accounted for in the data acquisition program. Since the number of sensors available in experiments are limited, a "divide and conquer" strategy is used to sweep the surface area of the structural component of interest. That is, during initial screening, accelerometers were evenly spaced so that they cover the entire surface. The areas that show the greatest damage metric were tested using a higher accelerometer density.

4.2 Data Processing

The methodology for mapping damage using a sideband-based damage index has been demonstrated using numerical simulations (Singh et al. 2017). However, the various practical aspects of the methodology have not been studied in the past. For example, the data collected in our experiments contains noise. In this section, we discuss data processing, noise reduction, and sideband detection techniques used in our laboratory experiments. We report on suitability of these methods for damage localization in structural components.

4.2.1 Calculation of the Damage Index

In our laboratory experiments, multiple accelerometers were placed on concrete specimens cured in an aggressive environment (60ºC and 100% relative humidity) to encourage ASR. The slab was excited using f_{pu} and f_{pr} frequencies, and the time history of accelerations is recorded at different locations on the surface of the slab. The PSD of the noisy acceleration time history was computed using the Welch's method (Welch, 1967) and a Nuttall-defined, 2048-point, four-term, symmetric, Blackman-Harris window (Nuttal, 1981). Note that the spectrum of the steady-state dynamic response of the structural component for a few cycles (6 to 8) of the pump signal is sufficient for successful sideband-detection (Singh et al., 2017). Thus, the overlap for the Welch's method can be decided based on the length (in time) of available data and the time period of the pump signal to ensure sufficient length of the signal is used to compute PSD. In our experiments, the length of the acquired signal contained about 180 cycles of the lowest f_{pu} (i.e., 920 Hz). Thus, we used the Welch's method with zero overlap. Linear spectrum (LS) of the acceleration time history was computed from the PSD (Figure 9). The nonlinearity in the structural response, or the modulation of the f_{pr} by the f_{pu}, is seen as sidebands around the f_{pr} ("peaks" in the LS at frequencies equal to $f_{pu} \pm f_{pr}$). After computing the LS, the values of AmpS1 and AmpS2 (Figure 9) were used to calculate the sideband sums (denoted as SBSum). It has been hypothesized that the effect of nonlinear structural behavior is pronounced near the site of damage (Singh et al. 2017). Thus, comparison of SBSum values at various locations can help in ascertaining the relative severity of damage (ASR-cracks) at these locations. In this report, we discuss mapping of ASR-induced cracks based on the SBSum metric, i.e., SBSum metric, $\mathrm{SBSum} = \mathrm{AmpS1} + \mathrm{AmpS2}$, as shown in Figure 9.

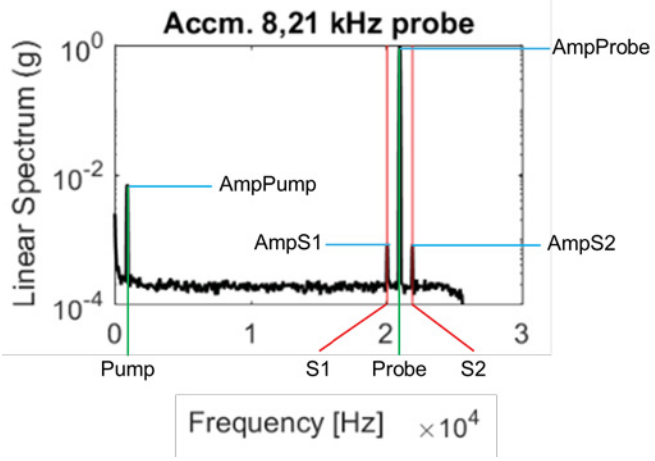

Figure 9. LS plot for an accelerometer labeled to show the values used in calculating SBSum. SBSum=AmpS1+AmpS2.

4.2.2 Baseline Adjustment for Sideband Identification

One of the key challenges in data processing was separating physically meaningful (nonlinearity-induced) sidebands (peaks) from noise-induced peaks at the specified frequencies ($f_{pu} \pm f_{pr}$) in the linear spectrum. For the experimentally collected data, the linear spectra in neighborhood of the sidebands do not show near-zero amplitudes at all sensor locations. Thus, an automated sideband detection algorithm may identify the *ambient* linear spectrum values at ($f_{pu} \pm f_{pr}$) as sidebands. Thus, the ordinates of LS at ($f_{pu} \pm f_{pr}$) need to be adjusted for the baseline value of LS in the neighborhood of sideband locations. Here, we subtracted the average of the LS ordinates in the neighborhood of the sidebands from the sideband values calculated from the LS (Figure 10). The regions where the mean noise was calculated are shown by green boxes in Figure 10. Thus, the peaks in the LS that correspond to the ambient noise are not counted as significantly high sideband values during data processing.

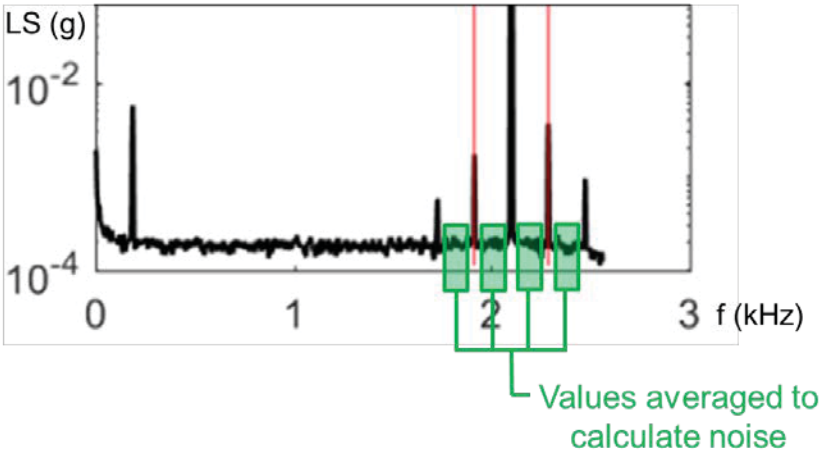

Figure 10. LS plot for a damaged structure. The red lines represent the sideband locations and the green boxes represent the window where the average of the LS was calculated.

4.2.3 Local–Maxima–Based Sideband Identification

The SBSum metric can be computed by finding the ordinate of the LS at given values of frequencies. Thus, an automated SBSum calculation process may be misled by considering ordinates at given frequencies that are not peaks (and hence do not indicate nonlinear structural behavior). To ensure that the values being used to calculate SBSum are physically meaningful sidebands, a method for finding local peaks in the data was implemented. In this method, it was first determined whether the sideband value for a given frequency was a local peak. Next, it was checked whether the sideband was a maximum value within a 1 kHz window (Figure 11) centered at the frequency of interest. The ordinate value at a given frequency was selected as a sideband only if it satisfies both the conditions given above.

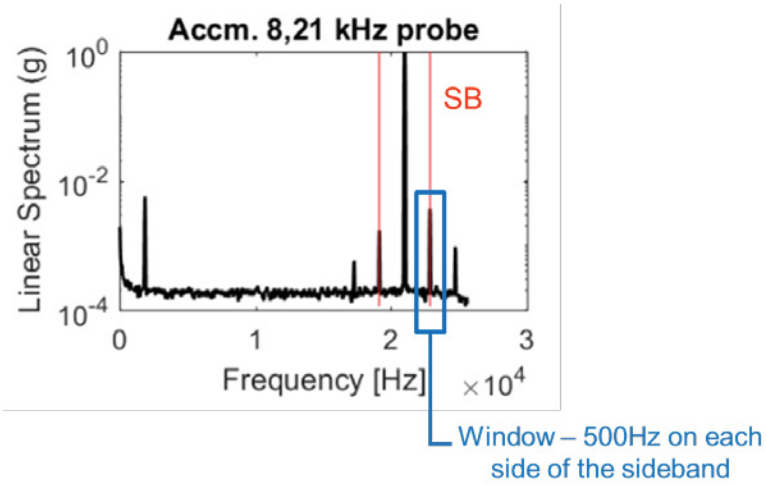

Figure 11. The blue box represents the 1000-Hz window being evaluated for local peaks for each sideband.

4.3 VAM Results

In this section, we report the results of VAM tests performed on the Vanderbilt University concrete sample and on the University of Alabama concrete samples.

4.3.1 VAM Results for the VU Slab

In this section, we report the results of VAM tests performed on the VU slab. In order to test the damage mapping capabilities of VAM-based diagnosis methodology, we divide the slab in four quadrants, and perform VAM test with a grid of 12 accelerometers for each quadrant. The pump and the probe actuators are placed adjacent to each other at the center of each quadrant (as shown in Figure 12). The blue circles and the green circle represent the pump and probe actuators respectively. We used different probing amplitudes (50, 100, 250, and 500 mV) and probing frequencies (17, 18, 19, 20, and 21 kHz) for VAM testing. The pumping frequency was 920 Hz with a 500-mV amplitude. We conduct VAM tests using these parameters for each quadrant, collect the acceleration time series data at each accelerometer location, compute the corresponding LS, and obtain SBSum metric using the methods detailed in Sections 4.2.2 and 4.2.3. Next, we plot the variation of the SBSum metric over each quadrant using linear interpolation of the SBSum metric obtained at accelerometer locations. We juxtapose damage maps for the four quadrants to obtain a damage map for the entire slab. Figure 13, Figure 14, and Figure 15 show damage maps for three probing frequencies.

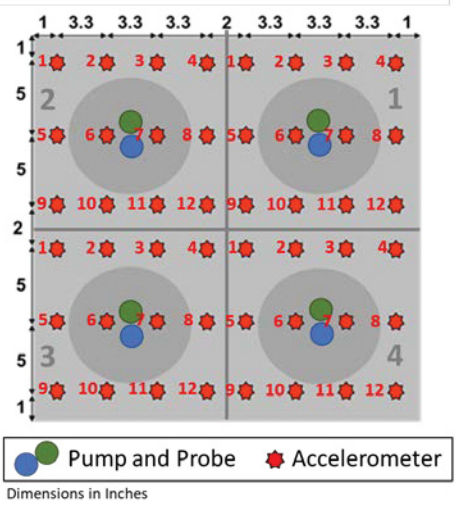

Figure 12. Pump, probe, and accelerometer locations for all four quadrant locations (labeled in gray).

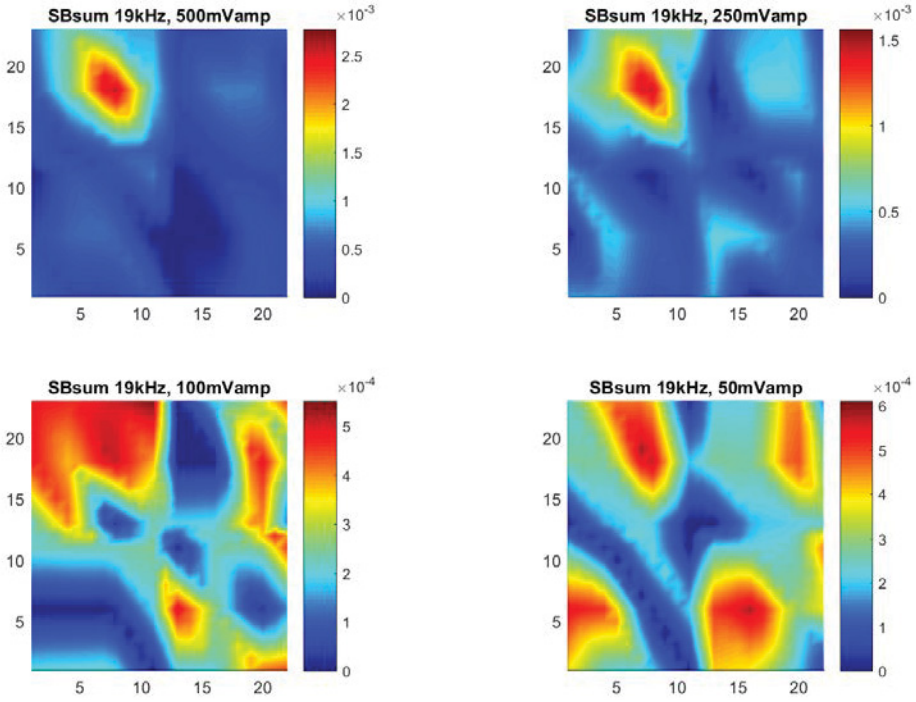

Figure 13. SBSum data in the LS of acceleration given a 500-mV pump of 920 kHz, and 500-, 250-, 100-, and 50-mV probes of 19 kHz for all four quadrant locations.

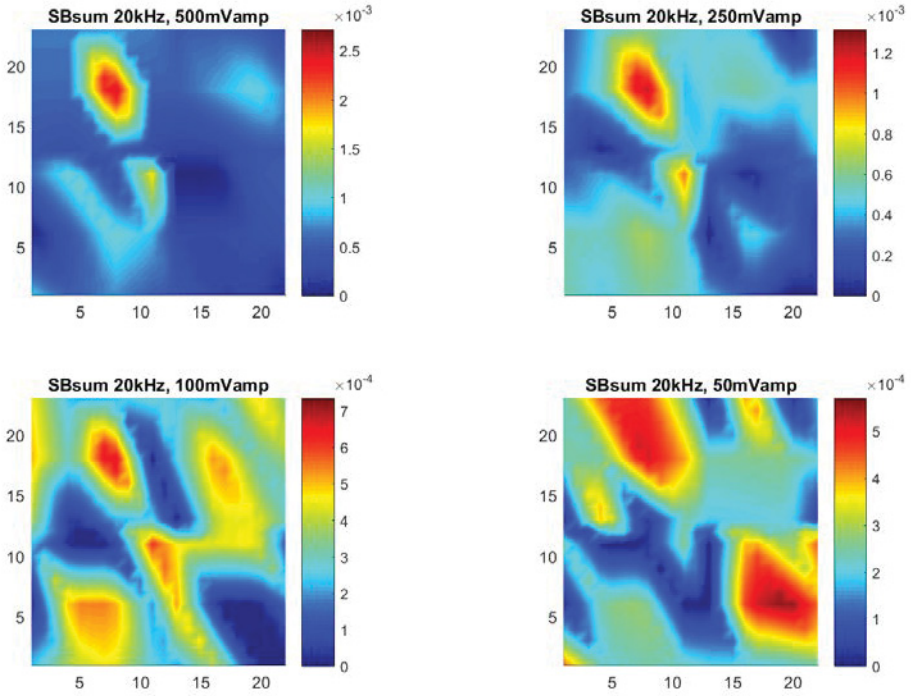

Figure 14. SBSum data in the LS of acceleration given a 500-mV pump of 920 kHz, and 500-, 250-, 100-, and 50-mV probes of 20-kHz for all four quadrant locations.

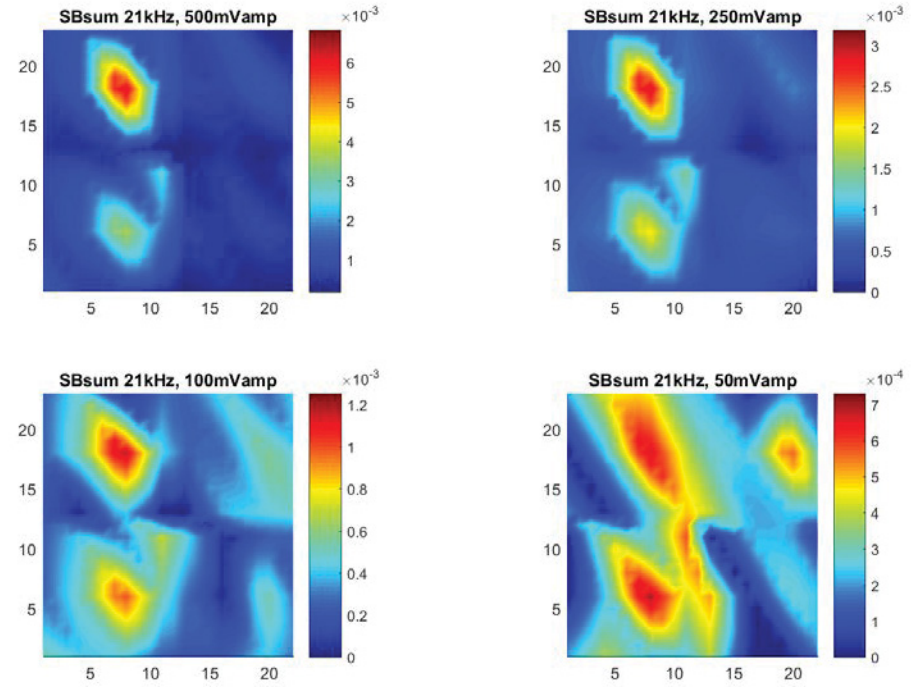

Figure 15. SBSum data in the LS of acceleration given a 500-mV pump of 920 kHz, and 500-, 250-, 100-, and 50-mV probes of 21 kHz for all four quadrant locations.

In Figure 13, Figure 14, and Figure 15, the locations of relatively higher SBSum values generally correspond to the locations of visible cracking in the slab. Since quadrant 2 contained pure silica, one of the main ingredients in the ASR gel, and showed two spots of degradations where the gel was seeping from the edges of the quadrant, we expect quadrant 2 to have the largest amount of ASR damage. This is indeed the case in Figure 13, Figure 14, and Figure 15, where quadrant 2 consistently has the highest value of the damage index (i.e., SBSum). We also expect a large amount of damage near the intersection of quadrants 3 and 4, since there is an area of effluent seepage. This is seen in low probe amplitude cases in Figure 13, Figure 14, and Figure 15.

Data analysis techniques are applied to better understand the results and the effects each variable has on the damage index (SBSum). The variation in the values of SBSum for different test parameters (location of the pump and probe actuators, probing amplitude, f_{pr}) can be displayed in the form of a scatterplot. A scatterplot shows the SBSum for every accelerometer for every test as a different point. The plots show visual correlations between high SBSum values and different test variables. These plots are shown in Figure 16, Figure 17, and Figure 18. In Figure 16, quadrants 2 and 3 show the highest values of SBSum. This supports the presumption of more ASR damage due to extremely reactive silica placed in quadrant 2. In Figure 17, the larger the probing amplitude was, the higher the SBSum values were experimentally. It is noted that, although a smaller f_{pu}/f_{pr} showed higher sideband values in these cases, it does not mean it enables better damage localization. Figure 18 shows the effects of probing frequencies on the SBSum. This plot shows the higher the probing frequency, the higher the SBSum values were for these experiments.

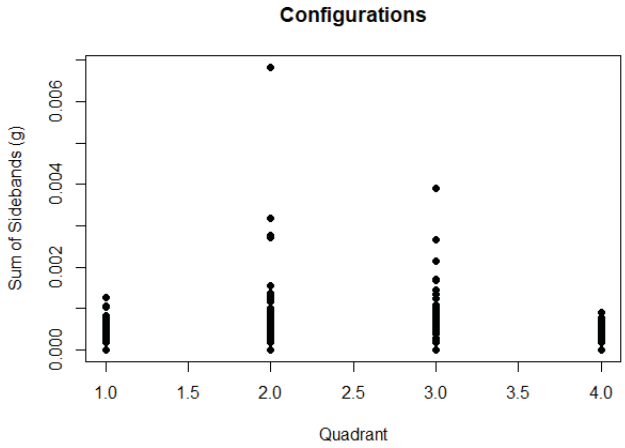

Figure 16. Scatterplot of the SBSum values for the configurations parameters each of the four quadrants.

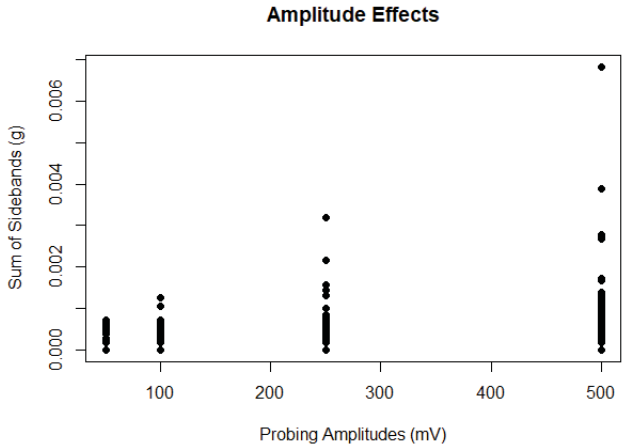

Figure 17. Scatterplot of the SBSum values compared to the different probing amplitudes.

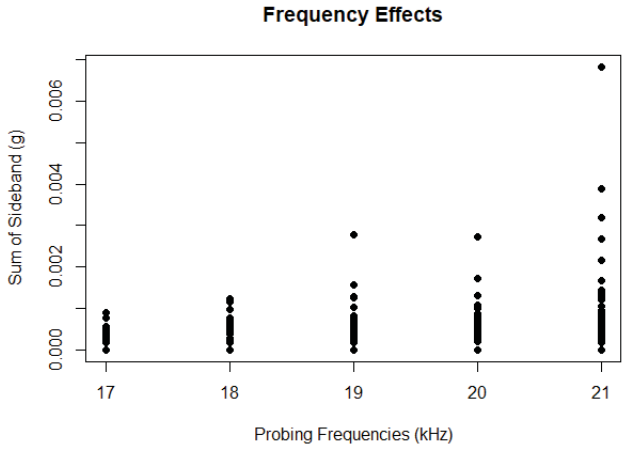

Figure 18. Scatterplot of the SBSum values compared to the different probing frequencies.

In Section 4.2.3, we described a method to select physically meaningful sidebands from noisy linear spectra by considering optimality in the neighborhood of the sideband locations as a filtering criterion. In this section, we show how the results are modified if this criterion is applied to select sidebands and to compute SBSum. The damage maps obtained using this method are shown in Figure 19, Figure 20, and Figure 21. Note that the VAM test parameters used in Figure 19, Figure 20, and Figure 21 correspond to those used in Figure 13, Figure 14, and Figure 15. Thus, a comparison of the two sets of damage maps (Figure 13, Figure 14, and Figure 15; and Figure 19, Figure 20, and Figure 21) shows the impact of the local-maxima-based filtering criteria. In these figures, quadrants 2, 3, and 4 show higher SBSum values for all probing frequencies.

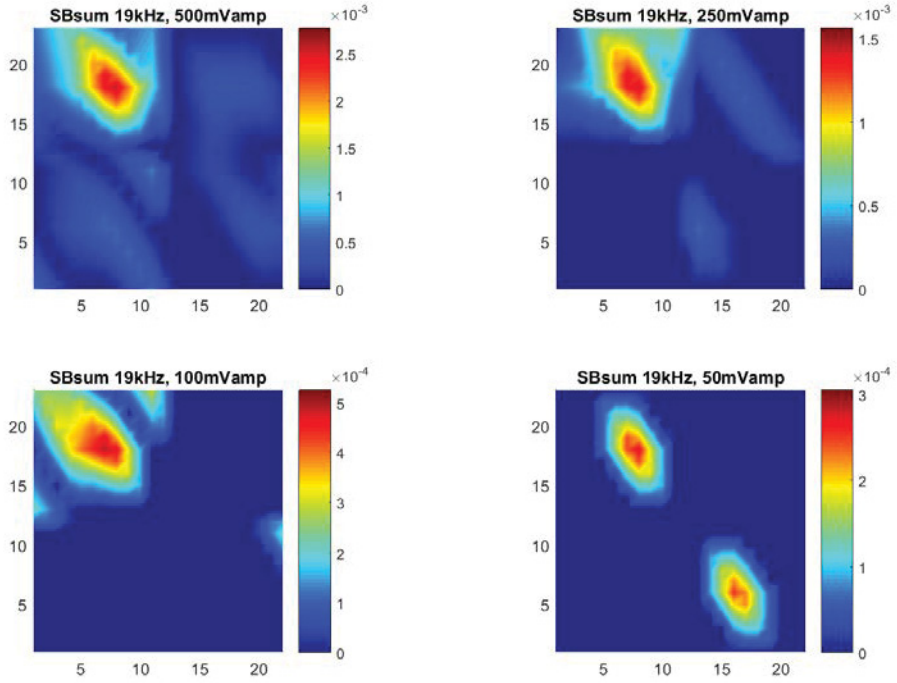

Figure 19. SBSum data in the LS of acceleration for local peaks given a 500-mV pump of 920 kHz, and 500-, 250-, 100-, and 50-mV probes of 19 kHz for all four quadrant locations.

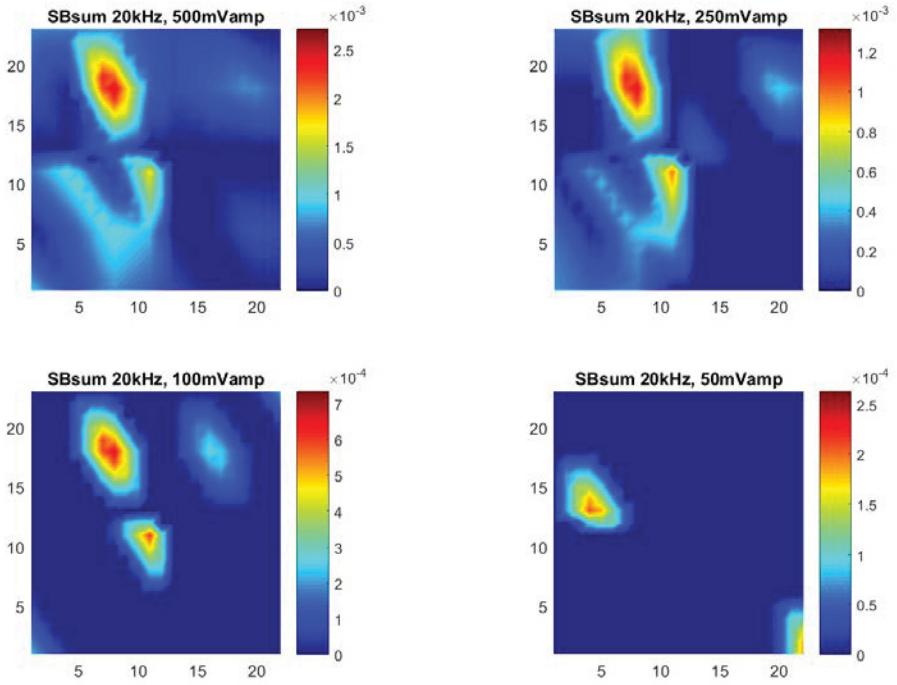

Figure 20. SBSum data in the LS of acceleration for local peaks given a 500-mV pump of 920 kHz, and 500-, 250-, 100-, and 50-mV probes of 20 kHz for all four quadrant locations.

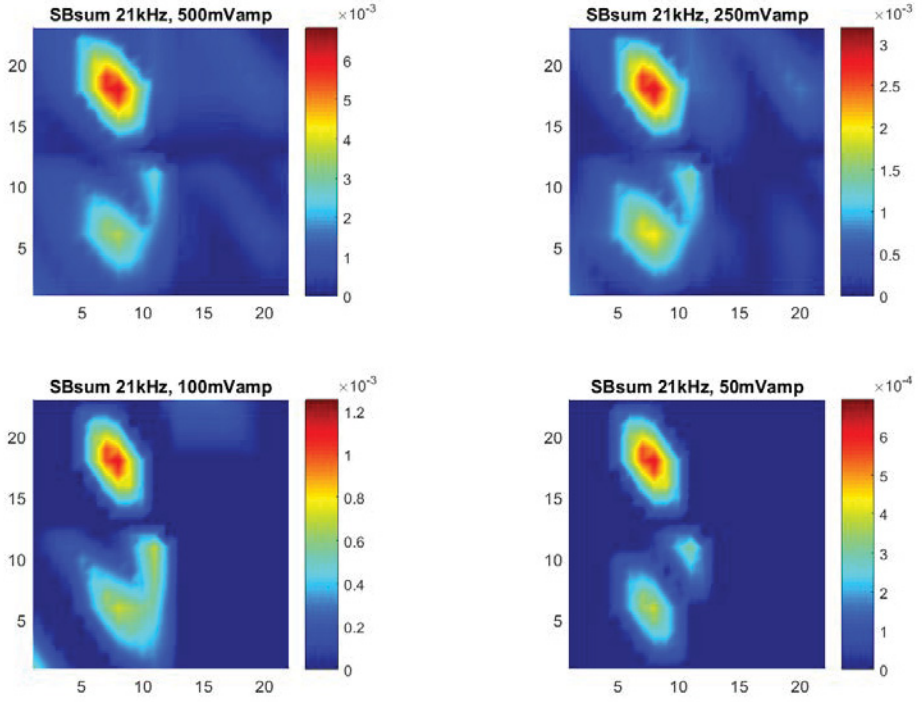

Figure 21. SBSum data in the LS of acceleration for local peaks given a 500-mV pump of 920 kHz, and 500-, 250-, 100-, and 50-mV probes of 21 kHz for all four quadrant locations.

4.3.2 VAM Results for the University of Alabama Slabs

In this section, we report VAM test results for four concrete slabs received from the University of Alabama. As mentioned in Section 3.2, two of the slabs were cast using reactive aggregate, and the remaining two slabs were cast using non-reactive aggregate. We perform VAM tests and we compare the magnitude of damage indices for slabs cast using reactive and non-reactive aggregate. We use a grid of 20 accelerometers for VAM testing of the Alabama slabs. Figure 22 shows locations of accelerometers as well as pumping and probing actuators. We perform the VAM test, acquire acceleration data for each pump/probe location, compute the damage index (SBSum) using the baseline adjustment method explained in Section 4.2.2, and sum the damage indices calculated for five sets of pump/probe locations for each half of the slab. We use linear interpolation to obtain damage index variation (damage map) over the top surface of the slab.

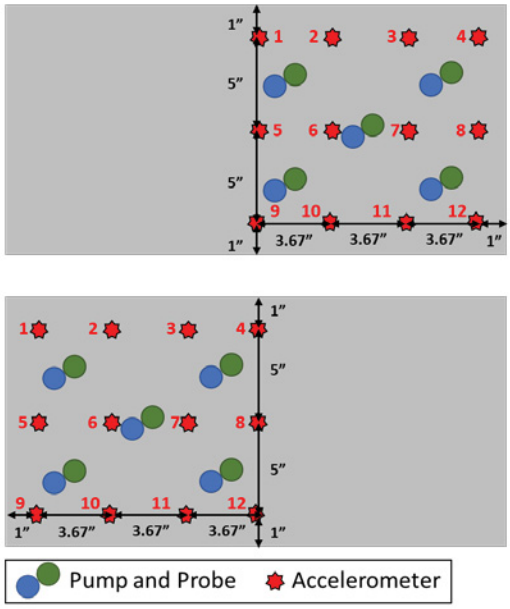

Figure 22. Accelerometer and pump and probe actuator placement for the University of Alabama samples.

The LS for acceleration shows high-magnitude sidebands for the reactive samples and no sidebands for the control (non-reactive) samples. This simple observation suggests that VAM tests can be used for detection of ASR damage in concrete. The reactive samples show surface cracking, whereas the control (non-reactive) samples for both Gold Hill and Grand Junction aggregates do not. Figure 23 and Figure 24 depict the LS plots of measured acceleration for the Gold Hill reactive and control (non-reactive) samples. The accelerometers are situated at the same locations (with respect to the centroid of the sample) on two different specimens. The magnitude and frequency for the pump excitation were 500 mV and 920 Hz, respectively, and those for the probe excitation were 250 mV and 21 kHz, respectively. Vertical red lines in all the plots indicate the abscissa (the possible locations) of the sidebands. It can be seen that high-magnitude sidebands are present the case of reactive slab. LS for acceleration for non-reactive slabs for both Gold Hill and Grand Junction aggregate samples do not, typically, show high-magnitude sidebands.

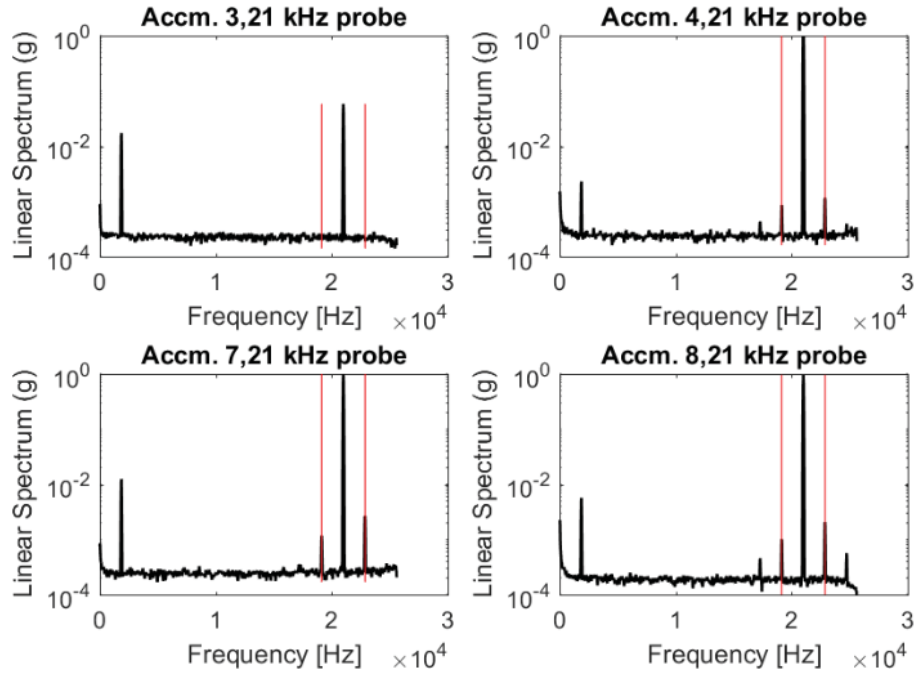

Figure 23. LS plots in terms of acceleration of the Gold Hill reactive sample with a 500-mV and 920-Hz pump and a 250-mV and 21-kHz probe for four different accelerometers.

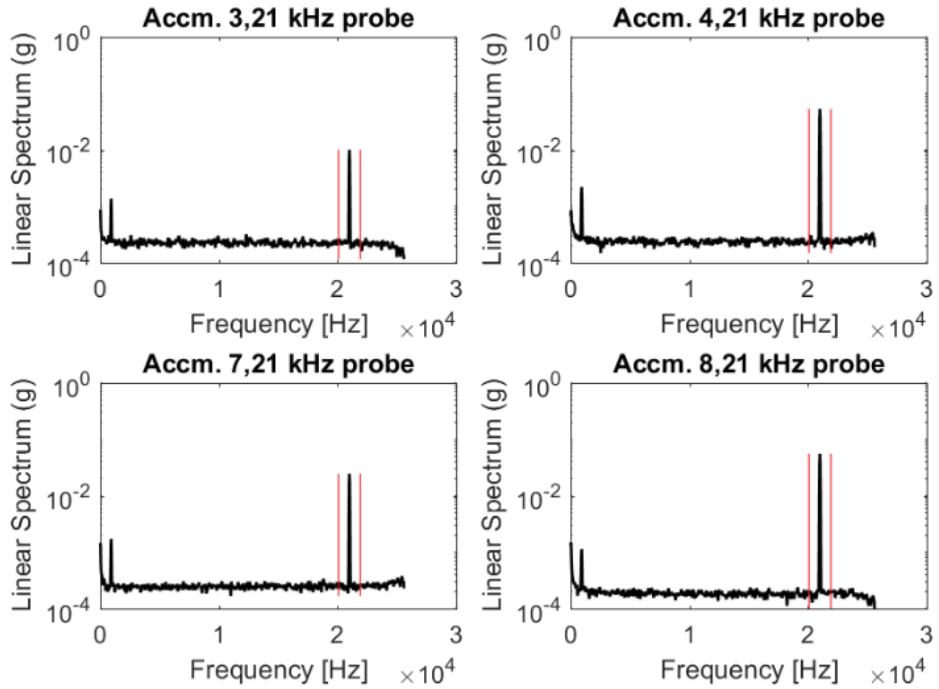

Figure 24. LS plots in terms of acceleration of the Gold Hill control (non-reactive) sample with a 500-mV and 920-Hz pump and a 250-mV and 21-kHz probe for four different accelerometers of the same location as shown in Figure 23.

We also performed the damage mapping for the University of Alabama samples using the method of filtering SBSum values explained in Section 4.2.3. Figure 25, Figure 26, Figure 27, and Figure 28 show damage maps for the pump magnitude of 500 mV, the pump frequency of 1695 Hz (Table 1), the probe frequency of 21 kHz, and four probe amplitude values (50, 100, 250, and 500 mV). The results for the Grand Junction reactive (Figure 25) do not show a consistent pattern for the distribution of SBSum values, and the SBSum magnitudes are similar to those observed for the Grand Junction control sample (Figure 26). The magnitude of SBSum in the Gold Hill reactive (Figure 27) is nearly ten times greater than that of the corresponding control (Figure 28). The Gold Hill reactive also shows consistently high sidebands for the same region for all probe amplitudes. In future work, this area will be further tested with a higher sensor density. The results for the reactive samples are more consistent for all probing amplitudes, whereas for the control samples, there is no consistency in the values of damage index at a particular region on the slab.

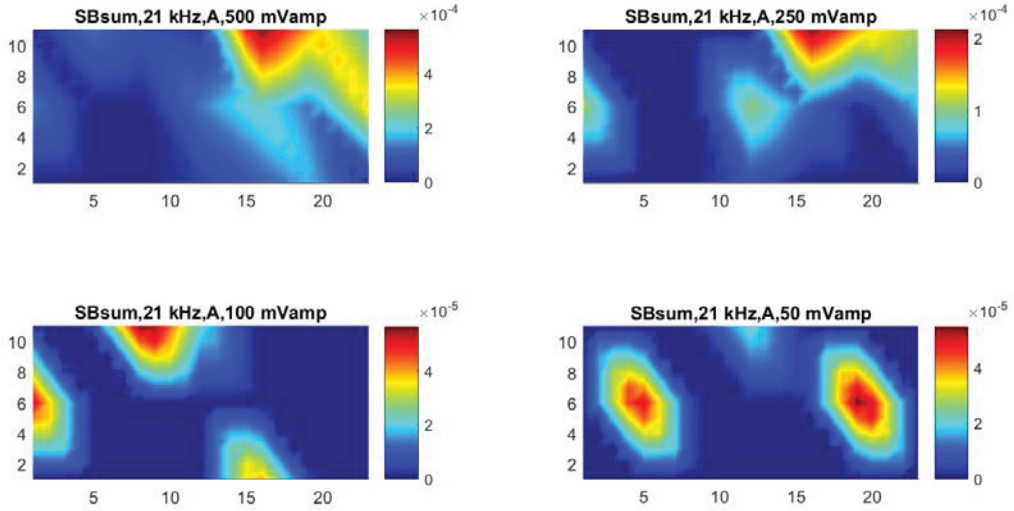

Figure 25. SBSum surface diagram for the Grand Junction reactive sample with a 1695-Hz and 500-mV pump and a 21-kHz probe of various amplitudes using a local peak filter.

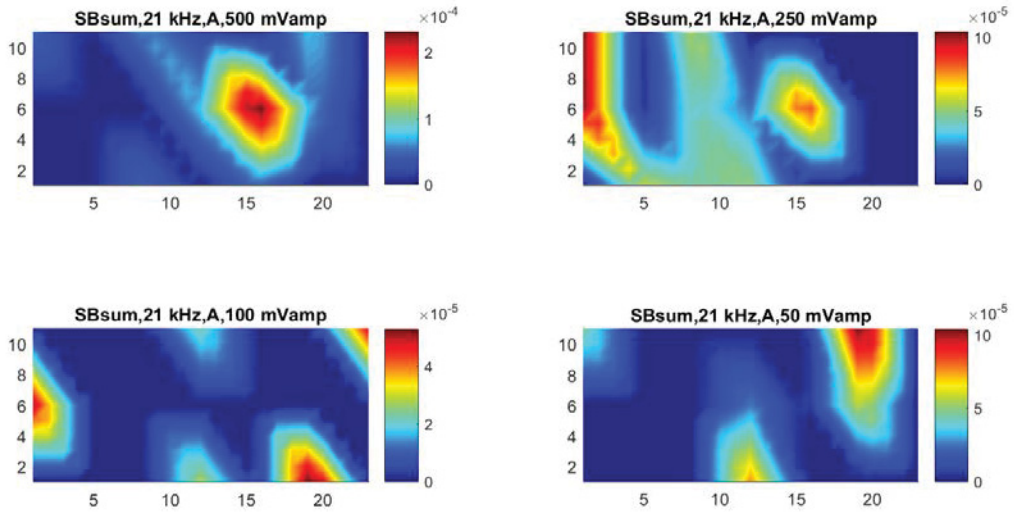

Figure 26. SBSum surface diagram for the Grand Junction control (non-reactive) sample with a 2240-Hz and 500-mV pump and a 21-kHz probe of various amplitudes using a local peak filter.

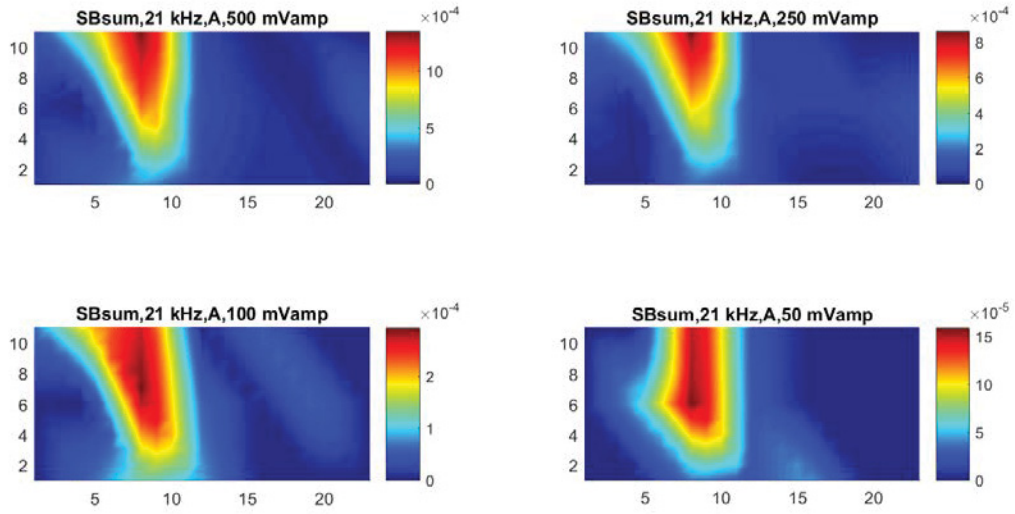

Figure 27. SBSum surface diagram for the Gold Hill reactive sample with a 1865-Hz and 500-mV pump and a 21-kHz probe of various amplitudes using a local peak filter.

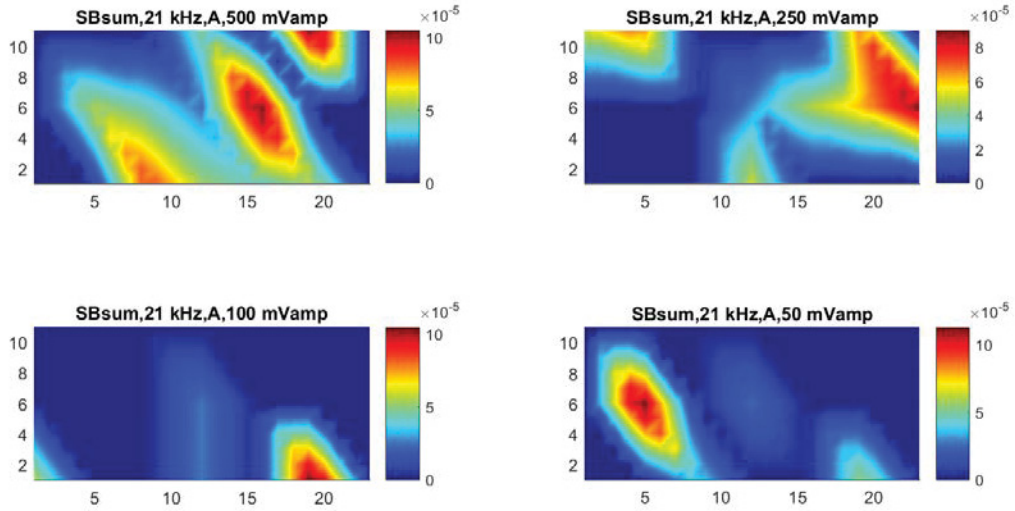

Figure 28. SBSum surface diagram for the Gold Hill control (non-reactive) sample with a 2390-Hz and 500-mV pump and a probe of various amplitudes using a local peak filter.

4.3.3 Summary of VAM Results

In this section, we discussed the results of our laboratory experiments aimed at determining the effectiveness of VAM tests for detection and localization of ASR-induced cracks in structural concrete components. We performed VAM-based diagnosis of a medium-sized slab containing pockets of reactive aggregates at known locations, as well as two sets of two slabs cast using either reactive or non-reactive aggregate (mixed throughout the slab). A damage index based on sidebands present in the LS of nonlinear dynamic structural response was used to map distribution of damage inside concrete slabs. We discussed some practical aspects of data processing and noise reduction involved in VAM testing for real structures. We found that the fundamental frequency of the structure (obtained using a hammer test) is the best choice for the pump frequency. For the medium-sized slab containing pockets of reactive aggregate at known locations, VAM-based damage mapping revealed damage signatures at locations that showed visible signs of ASR damage. The damage map also matched the expected extent of damage based on the

reactivity of aggregates (i.e., the damage index showed highest damage where pure silica was placed as aggregate). For a set of two slabs cast using either reactive or non-reactive aggregates (Gold Hill), the VAM test consistently showed higher sidebands for the slab containing reactive aggregate. For the same aggregate type (Gold Hill), the damage map consistently showed damage at the same location for various probe frequencies. For the other aggregate type (Grand Junction), the damage index for the reactive and non-reactive sample had approximately equal magnitudes, thus, the results of the VAM test were inconclusive.

4.4 Guidelines for VAM–Based ASR Damage Localization

With the experience and insights gained from the above VAM tests and data analysis, the following summarized guidelines are suggested to apply the VAM technique for the ASR damage detection and localization in concrete structural components.

4.4.1 Experimental Setup

Refer to section 4.1 for details of the steps below.

1) **Determination of Pumping Frequency (f_{pu}) (4.1.1)**
   - Instrument the structural component to be tested with a coarse grid of accelerometers.
   - Apply an impact (instrumented hammer hit) to the component and collect the time history of acceleration at each accelerometer.
   - Compute the power spectral density (PSD) for each time history and record the first peak of excitation in the PSD.
     - It should be approximately same for all accelerometers.
     - This is the estimated natural frequency the component to be used as f_{pu}.
2) **Determination of Probing Frequency (f_{pr}) (4.1.2)**
   - Select a few f_{pr} values ranging from 10*f_{pu} to 20*f_{pu}.
   - Conduct the test using these frequencies as f_{pr}.
3) **Sensor Layout (4.1.3)**
   - Place a coarse grid of accelerometers uniformly distributed on the surface of the sample.
     - In the data analysis 4.4.2 step 1, if none of the sensors show sidebands, shift the sensor grid.
4) **Actuator Locations**
   - Place the pumping and probing actuators as close together as possible.
   - Move the actuators to different locations across the surface of the component and re-test to ensure that all accelerometers receive sufficiently strong excitation.
5) **Actuator Amplitudes (4.1.3)**
   - Conduct a series of tests with different pumping and probing input voltages (in our experiments we used a probing amplitude of 1-, ½-, 1/5th-, 1/10th-times the input pumping amplitude).
   - Select the pumping-probing amplitude combinations where the pumping amplitude is much higher than probing amplitude in the linear spectrum of the displacement time histories (computed using the measured acceleration time histories).

4.4.2 Data Analysis

Refer to sections 4.2.1, 4.2.2, and 4.2.3 for details of the steps below.

1) Power Spectral Density

- Calculate the PSD using an overlapped segment averaging estimator such as Welch's method.
    - Set the window and overlap based on the time period of the pumping signal and the length (in time) of signals collected.

2) Linear Spectrum

- Calculate the linear spectrum plot of accelerations and displacements.
    - Check to see which tests have the probe amplitude about $1/10^{th}$ - $1/20^{th}$ of the probing amplitude in the linear spectrum of displacement. These are the tests to be used in further analysis.

3) Sideband Identification and Filtering

- Identify sidebands (ordinates) in the linear spectra at frequencies ($f_{pr} \pm f_{pu}$).
- Use the baseline adjustment method (4.2.2), and the local maxima method (4.2.3) to identify nonlinearity-induced sidebands.

4) Damage Metric

- Calculate the damage metric (SBSum or any other damage metric chosen for analysis) using filtered sidebands identified in step 3 above.
    - SBSum is the sum of the spectral value of the first and second sideband after filtering. $\mathrm{SBSum} = \mathrm{AmpS1} + \mathrm{AmpS2}$.
- Create scatter plots for the data showing the damage metric for different f_{pr}.
    - Chose the tests based on f_{pr} values that show high damage metric magnitudes for all actuator configurations.

5) Contour Plots

- Plot the contours of the damage metric for the selected tests over the surface of the tested sample.

Repeat experiment with a higher sensor density in the areas of damage.

5. DIGITAL IMAGE CORRELATION

The DIC technique was applied to the large concrete slab cast at UTK. DIC is a three-dimensional, full-field, optical NDE technique to measure contour, deformation, vibration, and strain. The technique can be used for many tests, including tensile, torsion, bending, and combined loading for both static and dynamics applications.

5.1 DIC Test Setup

An experimental setup for three-dimensional DIC and data analysis includes the following steps:

1. **Preparation**: Two cameras are mounted at either end of a tripod camera (base) bar so the relative position and orientation of the two cameras with respect to each other is known. A random or regular pattern with good contrast is applied to the surface of the test object. The initial imaging processing defines unique correlation areas, known as facets, that are defined across the entire imaging area and that typically range in size from 5 to 20 square pixels.

2. **Data acquisition and processing**: An image correlation algorithm tracks the movement of these facets by utilizing mathematical methods to maximize the similarity measures from successive images. The three-dimensional locations of each facet can be calculated. Full-field displacement data can be obtained by tracking these measurement facet points within the applied random (or regular) target pattern.
3. **Results**: Out-of-plane displacement (or deformation) map for the entire surface for each point in time, when the measurements are taken. Progression of expansion or relaxation of structure affected by various degradation mechanisms including the ASR, which can be calculated using the displacement maps taken at different times during the testing period or long-term operation.

As part of the inter-pathway collaboration within the Light Water Reactor Sustainability Program, Vanderbilt University is conducting research to investigate the monitoring of degradation in a concrete sample at UTK due to ASR using the DIC technique. A black-background-white-speckle pattern using acrylic latex paint was selected and applied to the slab. At the same time, the supporting fixtures for the DIC camera were also installed inside the environmental chamber. The technical basis for selecting optimal experimental settings are discussed in Neal et al. 2016.

One of the three slabs was allocated for monitoring using DIC, on a 2 × 2 ft square area on the top surface. The side view of the slab inside an environmental chamber is shown in Figure 29 and the DIC camera is shown in Figure 8. For DIC monitoring effort, a preliminary study was performed to determine the optimal speckle size and pattern and identify the most durable paints (Neal et al. 2016).

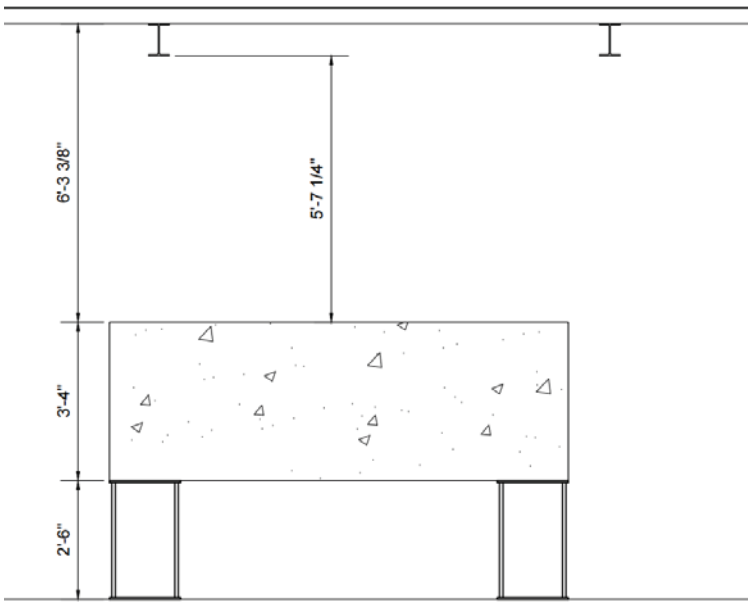

Figure 29. Side view of the slab at UTK.

5.2 Data Acquisition and Processing

The large mockup slab at UTK was studied using the DIC technique, every 2 months. After the acrylic latex paint was placed on the surface, visible degradation occurred over the course of the experiment. This was likely due to people stepping on the pattern and general movements on the slab surface during other damage evaluation tests. The pattern damage is visible as early as the second measurement set, as shown in Figure 30. By the third measurement set, the speckle pattern began to degrade in the upper and lower left-hand side of the painted area. The total percent loss of facets over the course of testing is noted in Section 4.3.3.

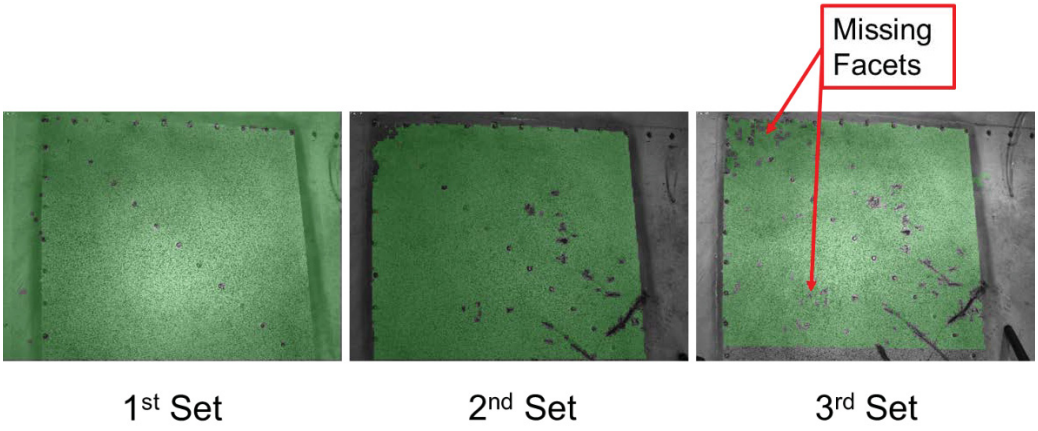

Figure 30. Degradation of the speckle pattern.

5.3 DIC Results

In processing the DIC information on the concrete specimen, each green square represented a facet (Figure 31). A facet is approximately 13 × 13 pixels. The relative motion between these facets is what allows the system to calculate the strain. The results for the DIC strain calculations are shown in Table 2, along with the date the tests were conducted and other variables. Figure 32 shows the plot for the average strains calculated using DIC in the X and Y directions over time. There is a large spike in the strain in both the X and Y directions during February 2017.

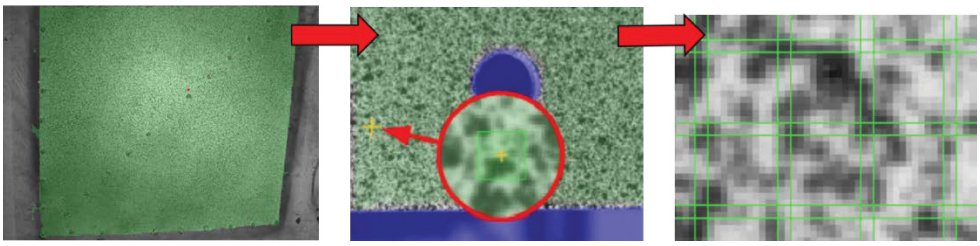

Figure 31. Pixel representation on the slab.

Table 2. DIC measurements taken bimonthly on the slab.

Date	Time of Meas.	Stage	Average Δεx (μm/m)	Average Δεy (μm/m)	Facets	Facet % Loss	T (ºC) Slab	Ambient T (ºC)
8/18/2016	1-2pm	0	---	---	15021	0	28.4183	---
10/17/2016	9-11am	11	1320	1090	14699	-2.14	38.2511	---
12/12/2016	9-11am	26	Bad Data	Bad Data	---	---	37.8926	---
2/17/2017	9-11am	31	2240	1930	14644	-2.51	36.7511	---
4/22/2017	9-11am	36	1780	1610	14545	-3.17	33.099	---
6/28/2017	9-11am	46	1750	1580	14683	-2.25*	37.8002	---
8/24/2017	9-11am	66	1700	1510	14706	-2.10**	23.9259	---
10/19/2017	9-11am	76	1620	1430	14532	-3.26	---	---
12/15/2017	9-11am	86	1650	1470	14605	-2.77	---	26.2

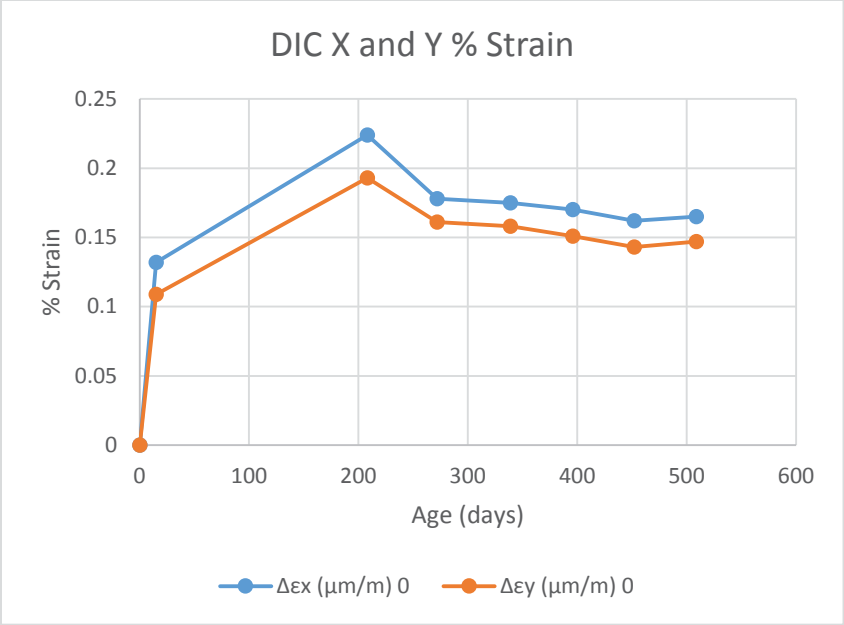

Figure 32. Plot of the average DIC strain in the X and Y directions over time.

To account for missing facets in the data and better understand what is occurring with the strain visually, post-processing methods are applied to the strain images. First, since the images are taking slightly at an angle, movement corrections are applied to remove stage-to-stage movements. Next, a mask is applied to remove edges and demountable mechanical strain gauge (DEMEC) studs from the figures and calculations. A filter is added that averages the strain for the facets over three runs using a 5 × 5 facet grid. Three-dimensional point interpolation was also applied to fill in missing points. The images were lastly scaled to only show strains with a 0 minimum to 3 sigma maximum.

The DIC results, namely strain distributions in the X and Y directions (along with the dates), are shown in Figure 33 and Figure 34, respectively. Figure 33 and Figure 34 show that DIC is effective in capturing the strain due to deformation in the large slab, caused by expansion with time. In addition, the color bars on the right of each image indicate the strain values corresponding to different colors, and also the frequency distribution of the strain values. In Figure 33, the normal strain in the X direction was zero everywhere in August 2016, then the average value increased to approximately 1150 μm/m in October 2016, and to approximately 1950 μm/m in February 2017. Similarly, in Figure 34, the normal strain in the Y direction was zero everywhere in August 2016, and then the average value increased to approximately 1250 μm/m in October 2016, and to approximately 2250 μm/m in February 2017. These results indicate that the large slab experienced significant expansion during the period from August 2016 to February 2017. Two issues were noted: (1) the data collected in December 2016 was unusable due to instrument malfunction; and (2) some damage to the speckle pattern was observed, as indicated by the white spots on the right-hand side of the diagonal (the white spots along the diagonal indicate the studs placed for visual measurement of deformation). The cause for the damage is suspected to be caused during the conduct of other NDE experiments on the slab. This damage and degradation of the facets has not affected the DIC results; the overall strain distribution is of importance and it is well captured by Figure 33 and Figure 34.

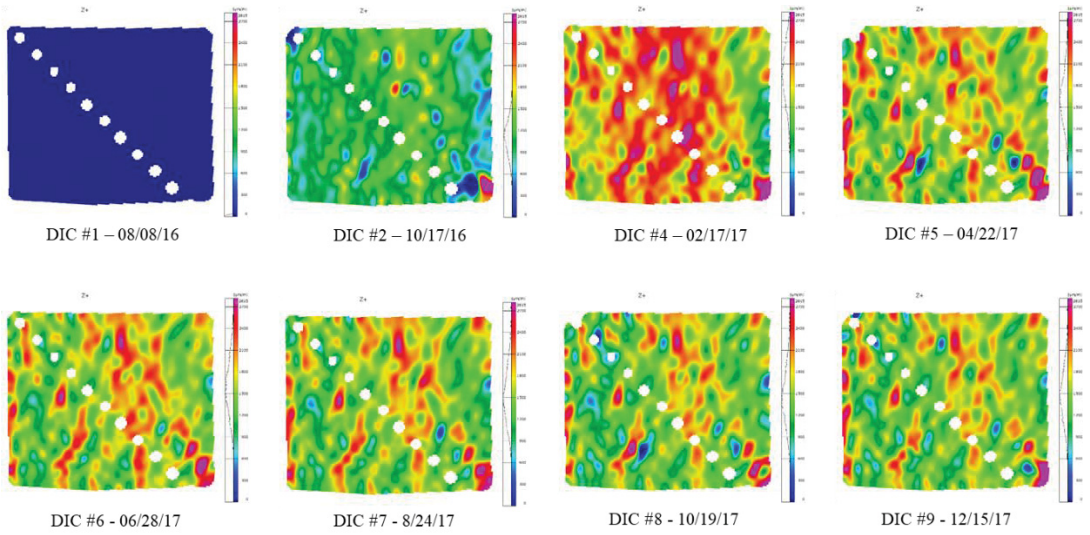

Figure 33. Strain distribution (normal strain in the X direction).

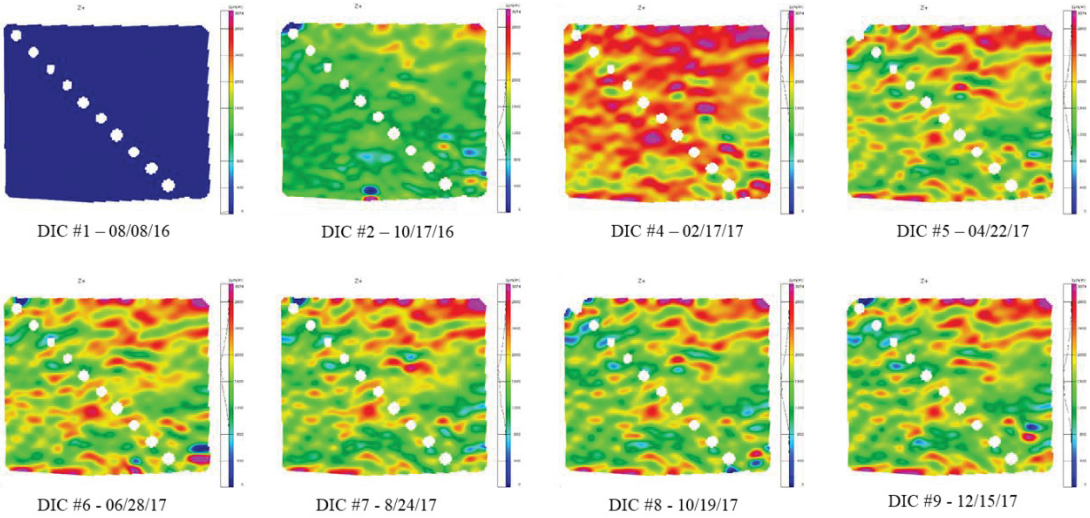

Figure 34. Strain distribution (normal strain in the Y direction).

For comparison with the strain data collected with the DEMEC gauges, Figure 35 shows the strain in the XY direction of the slab: normal to the direction of the DEMEC studs located on the XY axis. The average of the XY strain for the entire stage surface was equivalent to zero. For better comparison, only the strain values in between the DEMEC studs is analyzed. Figure 36 is a representation of the strain area between the DEMEC studs. The average values for strain in the X, Y, and XY directions between the studs are plotted in respect to time in Figure 37. The average strain in each direction between the studs follows a similar pattern as Figure 32, the plot for the entire stage surface.

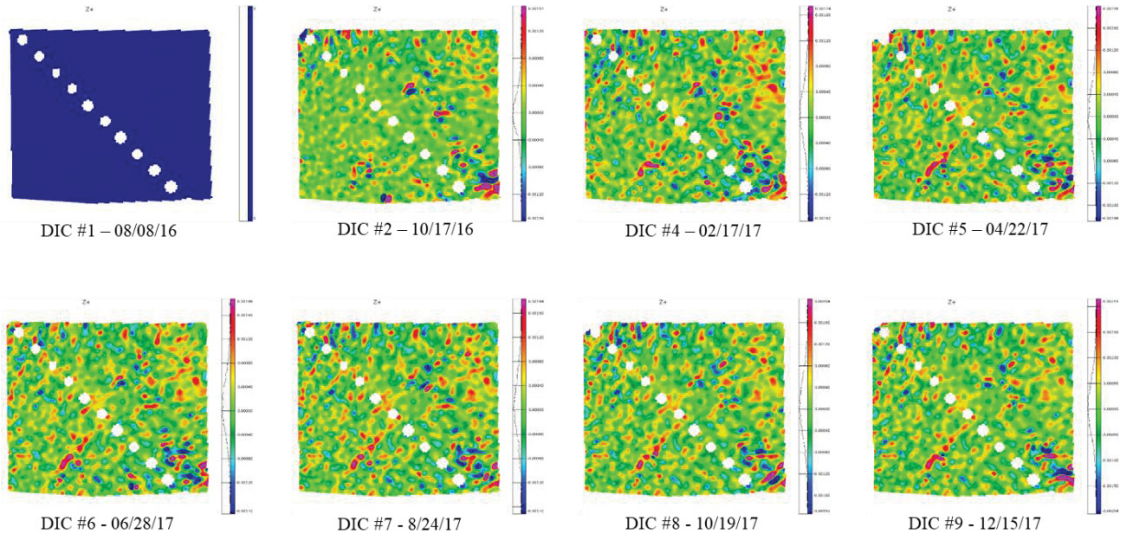

Figure 35. Strain distribution (normal strain in the XY direction).

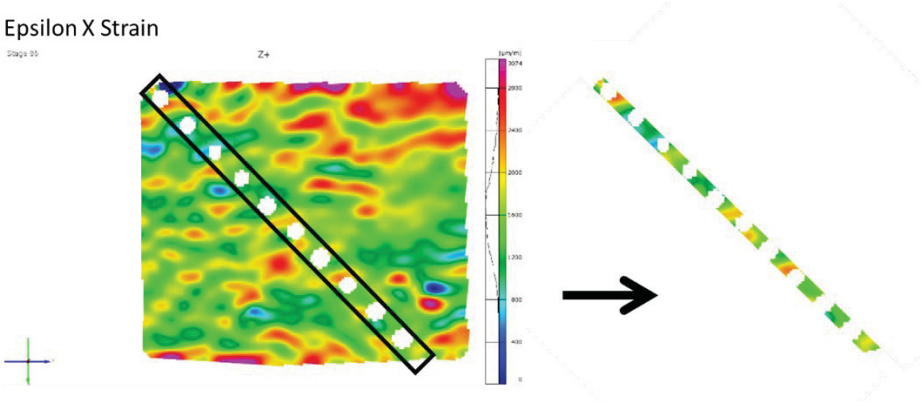

Figure 36. Visual representation of the facets used for the average calculations between the DEMEC studs.

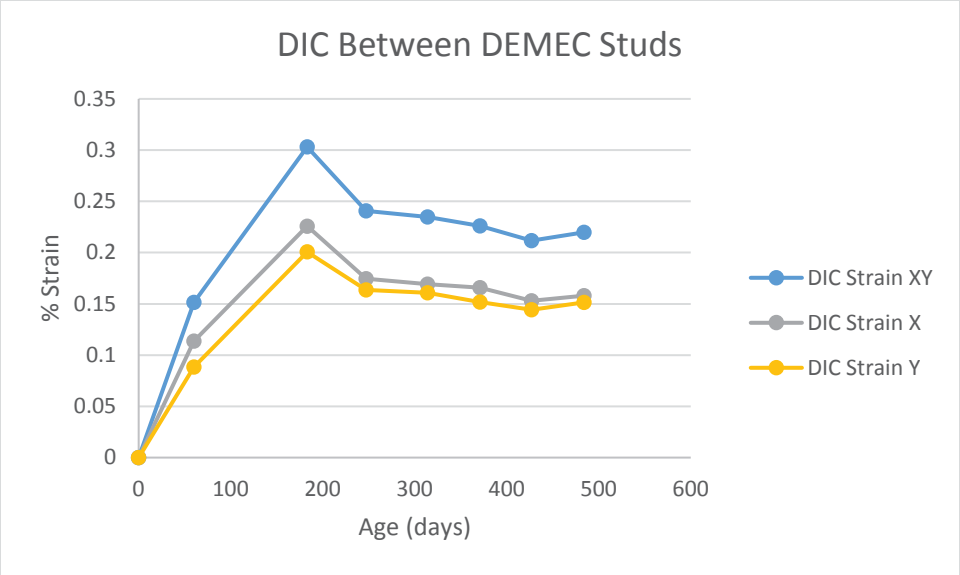

Figure 37. Average DIC strain values of the facets between the DEMEC studs.

DIC is a fast NDE technique to determine whether there is damage near the surface of a specimen. The technique is non-contact and full field: the image size is only limited by the standoff distance. There is no need for any pre-installed sensors or wiring and the pattern can be applied simply to a finished piece. A drawback of the technique is this pattern must remain on the part for the duration of the testing schedule. DIC also provides experimental data that directly is comparable to finite element simulation. When conducting DIC on the large ASR-induced slab, the average strain values in the X direction increased to approximately 1150 µm/m in October 2016, and to approximately 1950 µm/m in February 2017 and in the Y direction the strain values increased to approximately 1250 µm/m in October 2016, and to approximately 2250 µm/m in February 2017 before decreasing slightly and remaining constant for the following months. These results indicate that the large slab experienced significant expansion during the period from August 2016 to February 2017. After this time period the strain appeared to level out and remain consistent between acquisitions. As seen in Figure 33 and Figure 34, the distributions of strain remained relatively the same from April 2017 through December 2017. The strains recorded between the April to December 2017 tests decreased 7.3% in the X direction and 8.7% in the Y direction, respectively.

6. SUMMARY AND FUTURE WORK

The objective of this report was to examine the application of VAM and DIC techniques in assessing the effect of ASR on the integrity of concrete slabs that are exposed to the accelerated aging conditions in a laboratory setting. The VAM technique was applied to a 24 × 24 × 6 in. slab cast at Vanderbilt University with four pockets of reactive aggregates, and to four 24 × 12 × 12 in. slabs with reactive and non-reactive aggregates (dispersed throughout the slabs). The DIC technique was applied to a large concrete mockup at UTK. The main outcomes of the experiments and subsequent analyses include:

1. VAM successfully detected and localized the damage in the medium-sized concrete slabs from both Vanderbilt University and the University of Alabama. The occurrence of sidebands is dependent on the pumping and probing actuator locations, the two excitation amplitudes, and the two excitation frequencies. The performance of the technique was optimized by tuning the testing and signal processing parameters.
2. DIC was conducted on the large concrete slab at UTK. The results indicate that the large concrete slab experienced significant expansion during the period from August 2016 to February 2017 and has not experienced much change from April 2017 to December 2017.

Future work needs to focus on the following issues:

1. The VAM technique has in general shown good performance in terms of identifying the damage locations. Future work needs to focus on scaling up the technique to large-scale, field implementation of VAM-based diagnosis in NPP concrete structures. One of the key challenges is the number of sensors (accelerometers) needed. For a large structure, it is not feasible to use a large number of accelerometers; therefore, a remote-sensing full-field observation technique (such as laser vibrometry) might be beneficial. Another issue is the amplitude of the excitations to be applied in actual structures.
2. Scaling up VAM to realistic applications also requires the combination of computational modeling with experiments to further improve the damage localization. A related issue is the effect of uncertainty in diagnosis and prognosis, due to sensor noise, model uncertainty, and many other sources of concrete variability. Thus uncertainty quantification needs to be combined with VAM-based diagnosis and prognosis to develop a robust prognostics and health management framework.
3. Continue to monitor the large mockup at UTK using the DIC technique.

7. REFERENCES

Agarwal, V. and S. Mahadevan, 2014, "Concrete Structural Health Monitoring in Nuclear Power Plants," *Office of Nuclear Energy Sensors and Instrumentation Newsletter*, September 2014.

ASTM C1293-08b, 2015, "Standard Test Method for Determination of Length Change of Concrete due to Alkali-Silica Reaction," ASTM International, August 2015.

ASTM C1567-13, 2013, "Standard Test Method for Determining the Potential Alkali-Silica Reactivity of Combinations of Cementitious Materials and Aggregate (Accelerated Mortar-Bar Method)," ASTM International, 2013.

Bruck, P., T. Esselman, and M. Fallin, 2012, "Digital image Correlation for Nuclear," *Nuclear Engineering International*, April 23, 2012.

Chen, J., A. R. Jayapalan, J.-Y. Kim, K. E. Kurtis, and L. J. Jacobs, 2009, "Nonlinear wave modulation spectroscopy method for ultra-accelerated alkali-silica reaction assessment," *ACI Materials Journal*, Vol. 106, pp. 340–348.

Chen, X. J., J.-Y. Kim, K. E. Kurtis, J. Qu, C. W. Shen, and L. J. Jacobs, 2008, "Characterization of progressive microcracking in Portland cement mortar using nonlinear ultrasonics," *NDT&E International*, Vol. 41, pp. 112–118.

Christensen, J. A., 1990, "NPAR Approach to Controlling Aging in Nuclear Power Plants," *Proceedings of the 17th Water Reactor Safety Information Meeting*, Washington, D.C., NUREG/CP-0105, Vol. 3, pp. 509–529.

Kim, S., D. E. Adams, H., Sohn, G. Rodriguez-Rivera, N. Myrent, R. Bond, J. Vitek, S. Carr, A. Grama, and J. J. Meyer, 2014, "Crack detection technique for operating wind turbine blades using Vibro-Acoustic Modulation," *Structural Health Monitoring*, Vol. 13, No. 6, pp. 660–670.

Kreitman, K., 2011, "Nondestructive Evaluation of Reinforced Concrete Structures Affected by Alkali-Silica Reaction and Delayed Ettringite Formation," M.S. Thesis: University of Texas at Austin, Austin, Texas.

Ma, J., Z., S. Le Pape, N. Hayes, Q. Gui, A. Elhassan, and Y. Jing, 2016, Identification of Mechanisms to Study Alkali-Silica Reaction Effects on Stressed-Confined Concrete Nuclear Thick Structure, Oak Ridge National Laboratory, August 2016.

Mahadevan, S., V. Agarwal, K. Neal, D. Kosson, and D. Adams, 2014, *Interim Report on Concrete Degradation Mechanisms and Online Monitoring Techniques*, INL/EXT-14-33134, Idaho National Laboratory, September 2014.

Mahadevan, S., V. Agarwal, K. Neal, P. Nath, Y. Bao, G. Cai, P. Orme, D. Adams, and D. Kosson, 2016, *A Demonstration of Concrete Structural Health Monitoring Framework for Degradation due to Alkali-Silica Reaction*, INL/EXT-16-38602, Idaho National Laboratory, April 2016.

Mahadevan, S., S. Miele, K. Neal, Y. Bao, V. Agarwal, B. T. Pham, D. Adams, and D. Kosson, 2017, *Interrogation of Alkali-Silica Reaction Degraded Concrete Samples using Acoustic and Thermal Techniques to Support Development of a Structural Health Monitoring Framework*, INL/EXT-17-41852, Idaho National Laboratory, April 2017.

Naus, D., 2007, "Activities in Support of Continuing the Service of Nuclear Power Plant Safety-Related Concrete Structures," in *Infrastructure Systems for Nuclear Energy,* T. T. C. Hsu, C.-L. Wu, and J.-L. Li (eds), Chichester, United Kingdom: John Wiley & Sons, Ltd.

Neal, K., S. Mahadevan, V. Agarwal, G. Thorne, D. Koester, and B. T. Pham, 2016, *Digital Image Correlation of Concrete Slab at University of Tennessee, Knoxville*, INL/EXT-16-39921, Idaho National Laboratory, September 2016.

NextEra Energy Seabrook, 2012, "Impact of Alkali-Silica Reaction on Concrete Structures and Attachments," the Response to Confirmatory Action Letter, SBK-L-12106, from NextEra Energy Seabrook to the Nuclear Regulatory Commission (NRC), May 24, 2012.

Nuttall, Albert H. "Some Windows with Very Good Sidelobe Behavior." IEEE Transactions on Acoustics, Speech, and Signal Processing. Vol. ASSP-29, February 1981, pp. 84–91.

Singh, A. K., B. Chen, V. B. Tan, T. E. Tay, and H. P. Lee, 2017, "A theoretical and numerical study on the mechanics of vibro-acoustic modulation," *The Journal of the Acoustical Society of America*, Vol. 141¸ No. 4, pp. 2821–2831.

Ulm, F. J., O. Coussy, L. Kefei, and C. Larive, 2000, "Thermo-chemo-mechanics of ASR expansion in concrete structures," *Journal of Engineering Mechanics*, Vol. 126, No. 3, pp. 233–242.

Welch, P. D. (1967), "The use of Fast Fourier Transform for the estimation of power spectra: A method based on time averaging over short, modified periodograms", IEEE Transactions on Audio and Electroacoustics, AU-15 (2): 70–73